Development of a planning tool for cavity Photodynamic Therapy

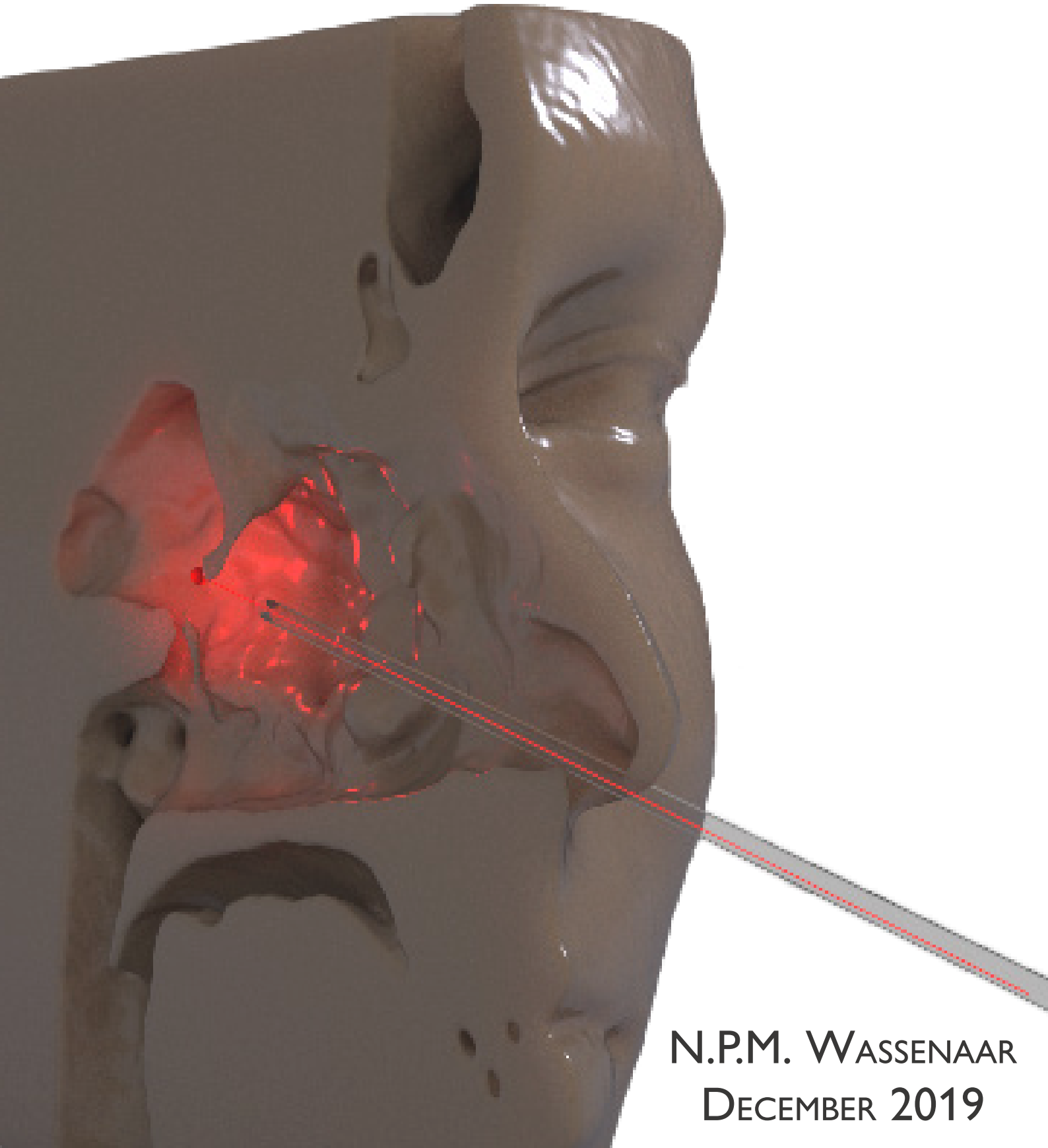

N.P.M. Wassenaar

December 2019

Master Thesis
Technical Medicine

N.P.M. Wassenaar

Head and Neck Oncology and Surgery
Verwelius 3D Lab
Netherlands Cancer Institute
University of Twente

Supervised by
Dr. Ir. F. van der Heijden
Dr. M.B. Karakullukçu
Dr. R.L.P. van Veen
Dr. M.J.A. van Alphen
Drs. B.J.C.C. Hessink-Sweep

UNIVERSITY OF TWENTE.

NETHERLANDS CANCER INSTITUTE
ANTONI VAN LEEUWENHOEK

Abstract

Background

Superficial sino-nasal carcinomas can be treated with cavity photodynamic therapy. This therapy is based on the use of a photosensitiser, oxygen and light of a specific wavelength to ensure tumour destruction. During photodynamic therapy, a red light source is placed inside the sino-nasal cavity of the patient to illuminate the tumour. However, not only the tumour cells are sensitive for red light, also the healthy cells will be damaged. Therefore, a planning is made prior to the therapy to decide location and output power of the light source resulting in tumour destruction and reducing the dose received by healthy tissue. The current planning method is mainly based on CT images and uses simple radiometric calculations to determine the incident light term and does not take scattering into account. The goal of this thesis is to develop a planning tool for cavity photodynamic therapy ensuring the best possible outcomes of the treatment.

Empirical light distribution model:

In previous research two models were developed to determine the light distribution in the sino-nasal cavity using the location of the light source and its output power. One model is based on the incident light term and the build-up function which calculates the contribution of scattered photons. Previous research found a linear relation of the build-up function, but this research showed that the build-up function can be described as a quadratic function. Furthermore, the relation between the build-up function and the characteristics of the cavity are assessed using spheres with a radius of 1, 2, 3 and 5 cm and reflection coefficient varied between 1, 50 and 99.9%. This research showed that a patient specific build-up function can be determined using the geometry of the cavity, the source location and the reflection coefficient.

Development of a planning tool:

A planning tool should be developed that a) automatically calculates the optimal source location and its output power which approaches a fluence rate at the tumour tissue between 80 and 120 mW/cm^2 and at the healthy tissue below 25 mW/cm^2 and b) provides the surgeon with 3D information on how the light is optimally distributed in the cavity. This problem is converted to a mathematical problem statement in the form of an objective function. The objective function is minimised using Grid optimisation and differential evolution. This research focuses on the optimisation of the objective function and the optimisation method. The most efficient optimisation method is determined based on the quality of the outcome, the computational speed and the reproducibility. Differential evolution is found to be more efficient than grid optimisation. The main drawback of the current optimisation is based on the light distribution models that are used. It is up till now not possible to take shaded areas into account and only the spherical bulb diffuser can be used. Therefore, the first steps towards the implementation of a microlens in the light distribution model are made.

Contents

List of Figures

List of Tables

List of Abbreviations

3D	Three dimensional
cPDT	cavity Photodynamic Therapy
CT	Computer Tomography
DA	Dual Annealing
DAMP	Damage-Associated Molecular Patterns
DE	Differential Evolution
EBV	Epstein-Barr Virus
EM	Electromagnetic
ENT	Ear, Nose and Throat
EPR	Enhanced Permeability and Retention
EUS	Endoscopic Ultrasound
FESS	Functional Endoscopic Sinus Surgery
HU	Hounsfield Units
HPV	Human Papilloma Virus
mTHPC	meta-Tetra(Hydroxyphenyl)Chlorin
OSL	Optimal Source Location
PDT	Photodynamic Therapy
PET	Positron Emission Tomography
PS	Photosensitizer
PSL	Possible Source Locations
RMSE	Root Mean Squared Error
ROS	Reactive Oxygen Species
SCC	Squamous Cell Carcinomas
SD	Standard Deviation
SHGO	Simplicial Homology Global Optimisation
SL	Source Location
TNM	Tumour, Node, Metastasis

1 Introduction

Residual or persistant superficial sino-nasal carcinomas can be treated with cavity Photodynamic Therapy (cPDT). The efficacy of cPDT mainly depends on the light dose that reaches the tumour tissue. Therefore, a planning should be made prior to the treatment to determine the best location and output power of the light source. This planning is currently not based on radiometric calculations, but mainly on intuition. The main goal of this thesis is to create a cPDT planning tool that is based on dosimetric calculations to ensure optimal tumour destruction and to reduce the side effects of cPDT.

In this first chapter, more information will be given concerning sino-nasal carcinomas and the principles behind photodynamic therapy (PDT). Furthermore, the problem statement will be defined. Chapter 2 focuses on the underlying physics of two light distribution models, the empirical and analytical model. The light distribution models can predict the distribution of light in the sino-nasal cavity using a spherical bulb diffuser.

Three different subjects are investigated in this thesis. The aim of the first subject is to improve the quality of the empirical light distribution model which is used in the cPDT planning tool. This research is described in chapter 3. Chapter 4 focuses on the second subject: the development and verification of the cPDT planning tool. Furthermore, the first steps towards the implementation of a microlens in the light distribution models is made in chapter 5.

Subsequently, the challenges to implement the cPDT planning tool in the clinical workflow are described in chapter 6. Future work suggestions are also given in this last chapter. Finally, an overall conclusion of this thesis is given.

1.1 | Anatomy

The nasal cavity and the four paranasal sinuses are air filled spaces in the skull. The nasal cavity is described as the space from the nasal ala (anteriorly) to the choana (posteriorly). Close to this nasal cavity are the four paranasal sinuses: the maxillary, frontal, sphenoid and ethmoid sinuses, see Figure 1.1. The names of these sinuses correspond to

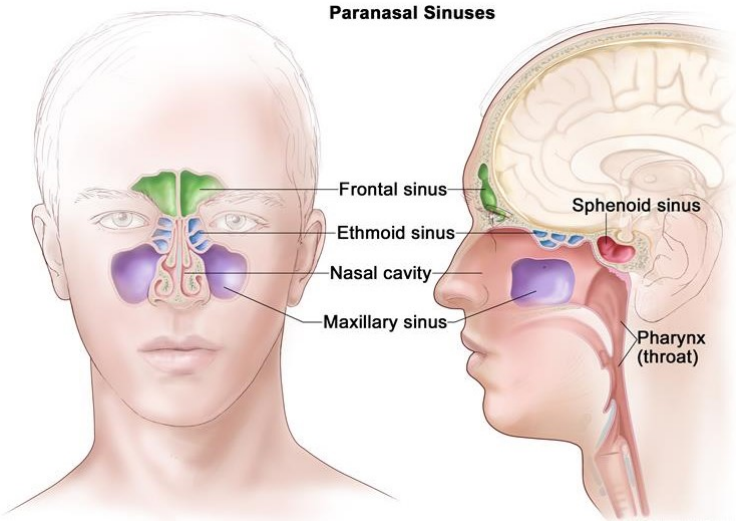

Figure 1.1: Anatomy of the nasal cavity and the paranasal sinuses [1].

the bones in which they are located. The maxillary sinus is the largest of the paranasal sinuses and is located laterally from the nasal cavity and inferior from the orbits. On the superior side of the orbits, the triangular shaped frontal sinuses are situated. The sphenoid sinuses are located posteriorly from the nasal cavity. Between the frontal and sphenoid sinuses, the ethmoid sinuses can be found. The ethmoid sinuses can be divided into the anterior, medial and posterior groups. All sinuses can drain into the nasal cavity via the middle or superior nasal meatuses that are situated between the conchae. The sinuses are formed by erosion of the nasal cavity in the surrounding bones and the size of the sinuses increase during life [1–4].

The exact function of the sinuses is not completely clear. However, it is assumed that the sinuses play a role in the immunological defence due to the production of antibodies and mucus. The sinuses also reduce the weight of the skull and they ensure humidification and heating of inspired air. Furthermore, the air filled spaces increase the resonance of the voice [2, 5].

1.2 | Sino-nasal carcinomas

1.2.1 | Epidemiology and aetiology

Tumours that occur in the nasal cavity and/or the paranasal sinuses are called sino-nasal carcinomas. Sino-nasal carcinomas are rare tumours, about five percent of all head and neck cancers are a form of sino-nasal malignancies [6]. In the Netherlands, about 124 patients were newly diagnosed with a form of sino-nasal cancer in 2017 [7].

Sino-nasal cancer is mostly diagnosed between the age of 50 and 70 and is more common in men than in women with a male-to-female ratio of 2:1 for Squamous Cell Carcinomas (SCC) [6]. The exposure to wood and leather dusts and various chemical substances play an aetiological role in the development of this type of carcinomas. The excessive use of alcohol, the exposure to tobacco smoke and a bad oral hygiene are also risk factors. Other important aetiological factors are the Human Papilloma Virus (HPV) and the Epstein-Barr Virus (EBV) [6, 8–10].

Sino-nasal carcinomas can develop from different types of cells that are present in the nasal and paranasal cavities. The most common type of sino-nasal carcinomas is SCC. Other types of these carcinomas are adenocarcinomas, adenoid cystic carcinomas, melanomas and esthesioneuroblastomas [10, 11].

1.2.2 | Diagnosis

The first clinical symptoms that arise due to a sino-nasal tumour are nasal obstruction, epistaxis and/or persistent rhinorrhoea. These symptoms are identical to other benign diseases of the nasal cavity or the paranasal sinuses such as sinusitis. This is why most of the sino-nasal tumours are diagnosed in an advanced stage. When the tumour has grown bigger, the patient can develop diplopia, proptosis and/or loss of vision. Furthermore, the tumour can extend into the oral cavity or into the brains which causes pain [6, 10, 12–15].

Physical examination of the head and neck area is essential to diagnose sino-nasal carcinomas. After inspection and palpation, a flexible endoscope can be used for visual intranasal examination. It is also important to make a Computer Tomography (CT) and Positron Emission Tomography (PET) scan to determine the extensiveness of the tumour and whether there are metastases or not. Sino-nasal carcinomas usually metastasise via the lymphatic system to regional lymph nodes, the lungs or the bones [16, 17]. When the location of the abnormal tissue is identified, a biopsy can be performed to determine its characteristics. This biopsy can be done under local anaesthesia at the outpatient clinic or during examination under general anaesthesia [14, 16].

1.2.3 | Treatment

There are different treatments available for sino-nasal carcinomas, such as surgery, radiotherapy, PDT or a combination of these. Which treatment option can be used, is determined per patient and is dependent on the characteristics of the tumour. Important decision factors are the size of the tumour and the presence of metastases [6].

Often a combination of surgery and radiotherapy is used. Surgery can be performed with an endoscopic resection, also called a Functional Endoscopic Sinus Surgery (FESS).

When the maxillary sinus is involved, one can choose to perform a maxillectomy: removing the whole maxillary sinus and the tumour. During surgery it is often impossible to remove the tumour radically due to the invasion of the tumour in the skull base, the orbits or other important structures. In this case, a combination of surgery and radiotherapy or surgery and PDT can be the best treatment option [6].

About 15 to 50% of all SCCs in the head and neck area will eventually recur. Treatment options for a recurrent disease is often limited. Radiotherapy can only be given once due to the side effects of the treatment on important organs like the brains. In contrast, PDT can be performed multiple times due to the relatively few side effects of the treatment [12–14].

1.2.4 | Prognosis

The five year relative survival lays between the 35% and 65% for all sino-nasal carcinomas. This prognosis is strongly dependent on the Tumour, Node and Metastasis (TNM) stage of the disease, the treatment options and the health state of the patient. Furthermore, smoking tobacco and consumption of alcohol will negatively influence the survival rate.The prognosis is also related to the HPV status, HPV-positive sino-nasal tumours generally have a better prognosis than HPV-negative sino-nasal tumours [9, 16].

1.3 | Photodynamic therapy

PDT is a minimally invasive procedure to treat superficial tumours. The therapy is based on photooxygenation reactions that are caused by a combination of a photosensitizer (PS), light and oxygen, see figure 1.2. The procedure can be divided into two stages: the administration of PS and the exposure to light. PDT can be used to treat different kind of tumours, like skin tumours, head and neck tumours, tumours of the digestive or urinary system and mesotheliomas [18, 19]. When PDT is used to treat tumours in the nasal cavity or paranasal sinuses, it is called cPDT.

1.3.1 | Photosensitizer

A PS is a molecule that ensures a chemical process after activation to a higher energy state. The PS can be activated by absorbing light of a specific wavelength. Currently, there are different PSs available for the treatment of head and neck carcinomas, with each its own characteristics. Temoporfin (Foscan®, Metatetra(hydroxyphenyl)chlorin (mTHPC), Biolitec Pharma, Dublin, Ireland) is currently used as PS at the Netherlands Cancer Institute (Amsterdam). Foscan® should be administered systemically via an

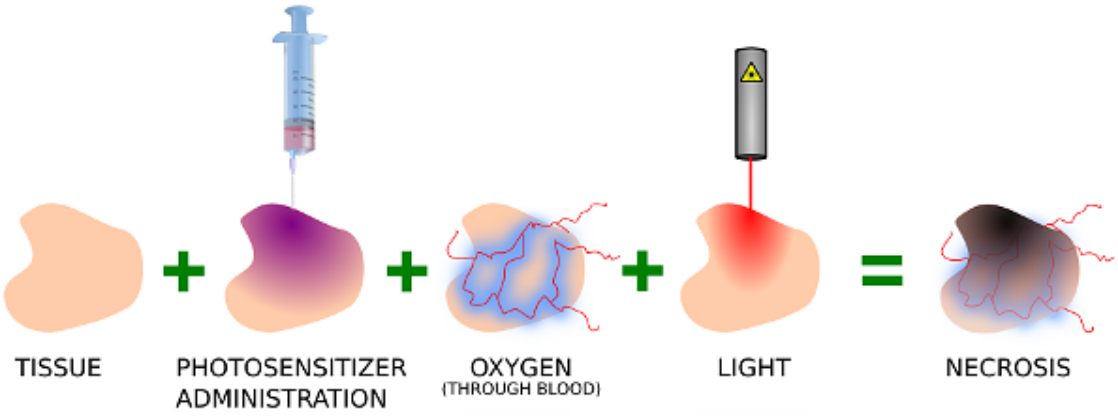

Figure 1.2: The three components that are needed to destruct the tumour: a photosensitizer, oxygen and light of a specific wavelength [20].

intravenous injection. The PS will spread through the body and will be stored in the cells. Accumulation of the PS will especially take place in the tumour cells due to the Enhanced Permeability and Retention (EPR) effect of the tumour as a result of poor lymphatic drainage and leaky vessels of the tumour. Enough PS should be accumulated inside the tumour cells to ensure a therapeutic effect of the treatment. For Foscan® this is the case after 96 hours [19, 21, 22].

1.3.2 | Light

When the PS is illuminated with light of a certain wavelength, photooxygenation reactions will take place. One of the optimal absorption wavelengths for Foscan® is 652 nm (red light) i.e. the visual wavelength at which the tissue penetration depth is high (8mm) [21]. When the PS is illuminated with this light, it will absorb a photon and will be promoted to its excited singlet state. The energy that is absorbed by the PS can be released in two different ways. First, the PS can release energy by emitting heat or via fluorescence and thereby going back to its ground singlet state. Second, the PS excited singlet state can turn into a triplet state T1. This triplet state T1 has a longer lifetime than the singlet state of PS. The triplet state T1 can also lose its energy using two different routes, called type I and type II, resulting in the toxic effect of the PDT procedure, see figure 1.3. In case of a type I reaction, the triplet state T1 transfers its electron to a substrate. This substrate becomes radical and can interact with molecular oxygen producing Reactive Oxygen Species (ROS). The type II reactions are defined by the transfer of energy to molecular oxygen and hereby producing reactive singlet oxygen [19, 21–23].

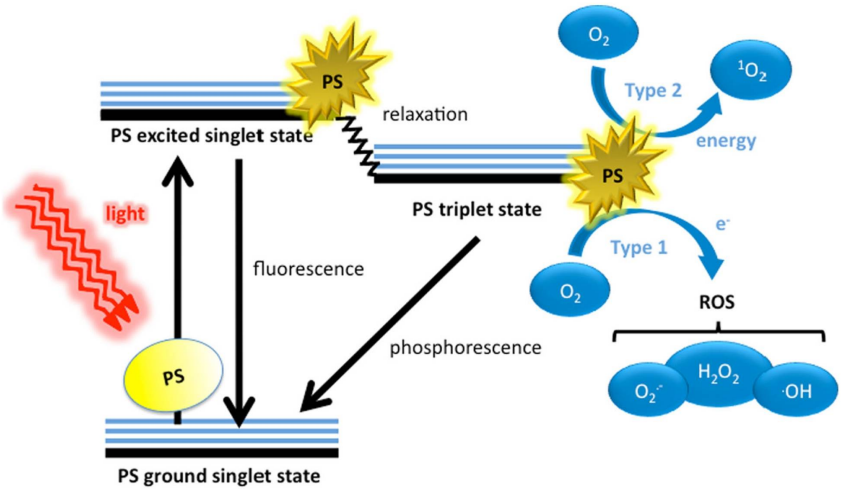

Figure 1.3: Schematic overview of the production of Reactive Oxygen Species (ROS) and singlet oxygen during PDT [24].

During cPDT, a light source is placed inside the sino-nasal cavity to illuminate the surface of the tumour tissue. Different light sources are available to illuminate the tumour: the cylindrical diffuser, the spherical bulb diffuser and the microlens, see figure 1.4. During the treatment with PDT, the light source that is able to fully illuminate the tumour is used. For example, the cylindrical diffuser is used for the illumination of the nasopharynx with a special designed nasopharynx applicator [25].

Tumour destruction during PDT will only take place if the tumour is illuminated with enough light. The light delivered to the tissue can be quantified in fluence (J/cm^2) or fluence rate (mW/cm^2). An optimal effect of the PDT using Foscan as PS will be reached when the fluence received by the tumour tissue is 20 J/cm^2. This dose should be delivered with a fluence rate of 100 mW/cm^2 during 200 seconds. When the fluence rate is too low, tumour destruction will not take place. Subsequently, the fluence should also not be too high to prevent rapid photobleaching. In case of photobleaching, the PS will change its structure causing an inability to transform to its excited state. Therefore, the photooxygenation reactions cannot take place and the tumour will not be destructed. Furthermore, the oxygen levels in the tissue can be depleted if the fluence is high. Earlier empirical research found that a fluence and fluence rate of respectively 20 J/cm^2 and 100 mW/cm^2 on the tumour tissue will lead to the optimal response. During the cPDT procedure, the position of the light source, the output power and the exposure time can be adjusted to ensure a maximum effect of the treatment [21].

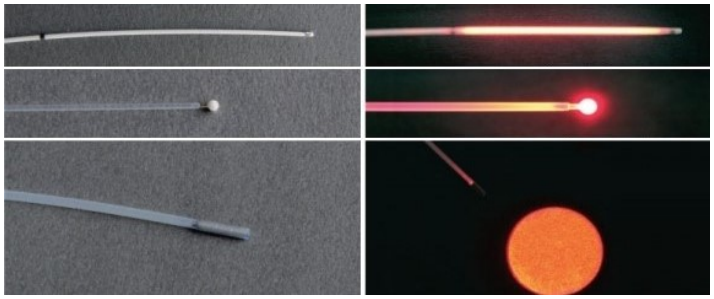

Figure 1.4: Different shapes of the light source that can be used during PDT: the cylindrical diffuser (top), spherical bulb diffuser (middle) and microlens (bottom) [26].

1.3.3 | Oxygen

The amount of oxygen that is present in the tumour tissue is important for the effectiveness of PDT. Photooxygenation reactions can only take place if enough oxygen is available in the tissue. As mentioned in section 1.3.2, two types of reactions can take place during PDT, type I and type II. Type II reactions will lead to the most tumour damage, but has a short lifespan (40 ns) and has a small radius of action (<20nm) [19]. Therefore, the place of accumulation of PS in the cell has a direct influence on the cell damage [22, 23].

During the treatment with PDT, the amount of oxygen in the tissue can differ over time. When the tissue is illuminated with a very high dose (fluence) during PDT, the oxygen levels in the tumour tissue can be depleted resulting in a limited effect of the PDT. Furthermore, when the tumour has a lot of hypoxic areas, the tumour can be resistant for the treatment with PDT [19].

1.3.4 | Mechanisms of tumour destruction

The photooxygenation reactions will lead to tumour destruction due to the production of ROS and singlet oxygen. The cells that are affected by these molecules will be destructed induced by apoptosis, necrosis or autophagy. Apoptosis is a controlled mechanism of cell death and will take place if the PS is localised in the mitochondria of the cells. When the cells are illuminated with a high fluence, cell death will most likely be induced by necrosis [18, 19, 27].

The working mechanism of PDT is not only based on directly induced cell death of the malignant tumour cells. PDT also affect the vasculature of the tumour by damaging the endothelial cells. When these endothelial cells are damaged, clotting factors will be released which subsequently leads to platelet aggregation, thrombus formation and vessel occlusion. Vasoconstriction will take place what eventually leads to tissue hypoxia and destruction of the tumour [19, 27, 28].

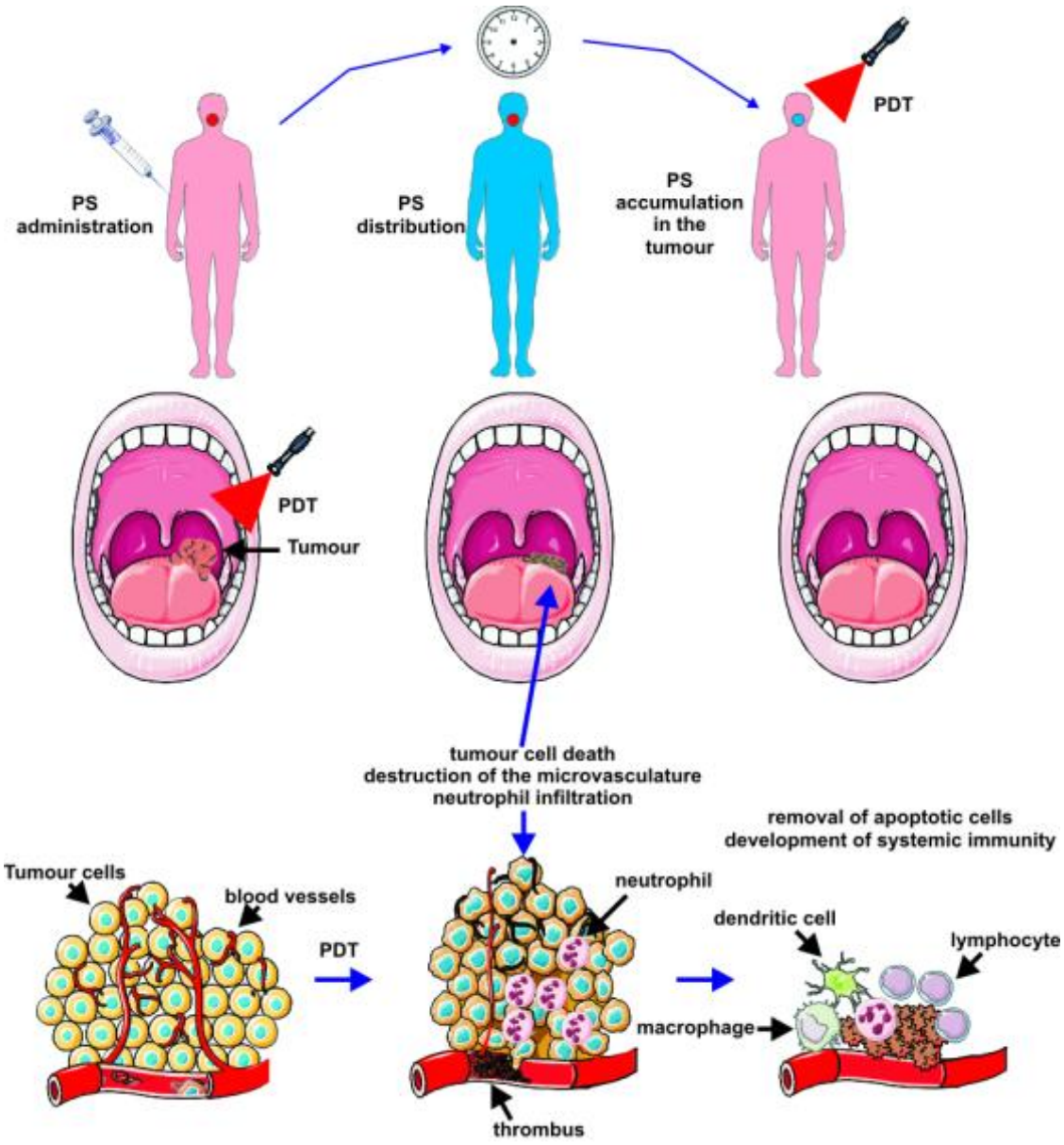

Figure 1.5: An overview of the working mechanisms of PDT. First, the PS will be administered to the patient, it will spread through the body and accumulate in the tumour. During PDT, tumour destruction will be induced in three ways: tumour cell death, destruction of the microvasculature and activation of the immune system [18].

Another mechanism of tumour destruction induced by PDT is activation of the immune system. Oxidative stress and cell death can result in release of inflammatory cytokines and damage-associated molecular patterns (DAMPs). Various white blood cells, neutrophils and macrophages are stimulated and will migrate to the illuminated cells. The damaged cells are phagocytised by the macrophages and specific proteins will be presented to T-helper cells which will activate cytotoxic T-cells. The immune system will also be active after PDT and not only during PDT. Tumour cells present in the body after PDT will be induced by cell death due to the immune system. An overview of the working mechanisms of PDT is shown in figure 1.5 [19, 27, 29, 30].

1.3.5 | Side effects of PDT

Unfortunately, there are also some side effects of PDT. Despite the accumulation of PS in the tumour, the PS is also present in the healthy tissue of the patient. Therefore, after administration of the PS the patient is sensitive for light. The patient should take precautionary measures by following a strict ambient light exposure plan to avoid direct light contact especially direct sunlight. Severe burn wounds, redness, blistering or skin necrosis can occur if the skin is overexposed to light [21, 28].

Furthermore, the patient will experience a lot of pain after the treatment. Sometimes it is difficult to manage the pain. This pain is caused by necrosis and swelling of the treated area. If the target area is located near, for example the dura or the optic nerve, damage to these structures can occur. Other side effects are infections, anaemia, dizziness or allergic reactions [21, 28].

1.3.6 | Current workflow of cPDT

The cPDT procedure is performed about 10 times a year at the Netherlands Cancer Institute in Amsterdam. The tumour should meet some requirements to be able to treat it with cPDT. The most important requirement is the depth of the tumour. The penetration depth of light in tissue is only 5 to 15 mm for wavelengths between the 630 and 700 nanometer and depends on the optical properties of the tissue. The tumour depth is measured on the endoscopic ultrasound. PDT can be effective if the tumour is thinner than four millimetre [28].

If the tumour is too thick to be treated with cPDT, a surgical debulking procedure (FESS) can be considered. As much as possible volume of the tumour will be removed during FESS. The tumour will be thinner and can therefore be treated with cPDT. This will only be effective if it is performed when the area, that is treated with debulking, is healed (about six weeks later). Extra vascular blood will reduce the amount of light that reaches the tissue and will therefore interfere with the cPDT, reducing the effects of the treatment [28].

Next to the depth, the surgeon will assess the location of the tumour. If the tumour lays too close to vital structures like the optic nerve, PDT will lead to many side effects. These side effects will deplete the quality of life of the patients and do therefore sometimes outweigh the advantage of treating the tumour with cPDT [28].

If it is possible to treat the tumour with cPDT, a patient specific cPDT light dosimetry plan is made. This planning should be made to ensure a sufficient fluence on the tumour cells and concurrently to limit the fluence on the healthy cells. The location and the output power of the light source that ensure the best outcome should be determined. Nowadays, a planning is made by scrolling through the CT scan of the patient and choosing the location and output power of the light source intuitively without taking scattering into account. When the planned location is reached during cPDT, the light source is fixated and it will illuminate the cavity for 200 seconds with the planned output power. An isotropic measuring probe is also placed inside the cavity to check if the desired fluence is reached with the planned location and output power of the light source.

1.4 | Problem statement and goal

The response of the tumour to cPDT is dependent on the light dose that is delivered to the tumour tissue. If the tumour receives a low fluence, the effect of the treatment will be limited. Subsequently, the fluence should also not be too high to prevent rapid photobleaching. A fluence and fluence rate of respectively 20 J/cm^2 and 100 mW/cm^2 on the tumour tissue will lead to the optimal response [21]. The fluence rate on the healthy tissue should be kept to a minimum, preferably below 25 mW/cm^2, to prevent damage to the healthy tissue.

The fluence reaching the tumour depends on the distance from the light source to the tumour and on the output power of the light source. Using the current workflow, the characteristics of the light source are determined prior to the treatment. However, this planning method lacks accuracy, because it is mostly based on intuition and not on dosimetric calculations. Therefore, it is difficult to ensure the same quality of cPDT treatment for every patient. When the planning prior to the treatment is more accurate, the effectiveness of the treatment could be improved.

The main goal of this study is to develop a light dosimetry planning tool for the treatment of superficial sino-nasal carcinomas with cPDT. The development of a cPDT planning tool will be based on a model that is able to calculate the light distribution in a sino-nasal cavity. A first light distribution model has already been developed in earlier research by Van Doeveren et al. and Bouwmans et al. [31, 32]. The first sub-goal of the current study is to improve the quality of the empirical light distribution model. The second sub-goal is to develop an optimisation algorithm that is able to calculate the

optimal light source location (OSL) and its corresponding output power. This should result in a cPDT planning tool which can be used to automatically calculate the best possible settings during the treatment.

2 Light distribution models

The planning tool for cPDT is based on an algorithm that calculates the light distribution in a sino-nasal cavity. At the Netherlands Cancer Institute, two light distribution models were developed, an empirical and an analytical model [31]. Both models calculate the fluence rate at each face of a triangular mesh that represents the sino-nasal cavity of the patient. With the location and the output power of the light source, the light distribution in the cavity can be calculated. To be able to understand the working mechanisms of both models, some background about the radiometric basics of tissue optics is elaborated. After that, the analytical and empirical model are discussed in detail.

2.1 | Triangular mesh

Three dimensional (3D) objects can be described with vertices and faces, see figure 2.1. Vertices are 3D coordinates of points in space which describe the location of the object. The vertices are connected to each other by faces. These are triangular shaped planes that describe the surface of an object. The sino-nasal cavity wall can be described in 3D using these vertices and faces. Such a 3D representation of an object is called a triangular

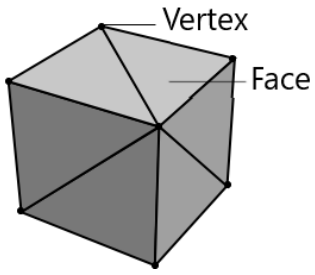

Figure 2.1: Triangular mesh of a cube consisting of vertices and faces.

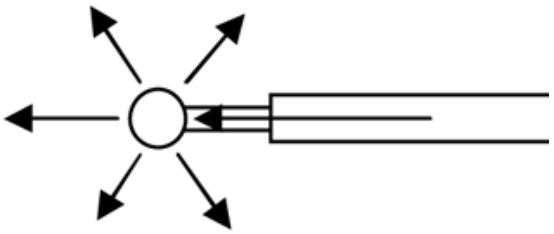

Figure 2.2: Schematic representation of the spherical bulb diffuser [33].

mesh. The light distribution models, that will be described in this chapter, are able to calculate the light distribution in a sino-nasal cavity that is divided into faces. The light distribution models will give the fluence rate that reaches each face of the triangular mesh.

2.2 | Radiometric basics of tissue optics

As mentioned previously in section 1.3.2, different light sources can be used during cPDT. The light distribution models that are described here are based on the spherical bulb diffuser (Medlight SA, Ecublens, Switzerland), see figure 2.2. The light source emits photons into the cavity and ensures illumination of the cavity wall. Each light source has its characteristic manner of distributing the light through the cavity. The fluence rate on the surface of the cavity is the sum of the incident light and the back scattered light from surrounding faces. The incident light can be described as the amount of photons that reach a certain point in space direct from the light source. When an isotropic spherical bulb diffuser is used, the incident light that reaches a certain point in space can be calculated with equation 2.1.

$$\phi_{inc} = \frac{S}{4\pi r^2} \tag{2.1}$$

Where ϕ_{inc} is the fluence rate of the incident light at the point in space, S is the output power of the light source and r is the distance between the spherical bulb diffuser and the point in space.

Equation 2.1 cannot be used to calculate the fluence rate that is received by a plane. The fluence rate will spread over the surface of the plane and the fluence rate at each point is therefore dependent on the angle between the incoming incident light beam and the normal of the plane. According to this, the angle should be implemented in equation 2.1 to be useful for the calculation of the incident fluence rate at each face of the triangular mesh. However, the fluence rate in the sino-nasal cavity is measured using an isotropic measuring probe. The amount of fluence rate that is measured does not depend on any angle. The light distribution models that are developed, try to simulate the fluence rate that will be measured by an isotropic measuring probe. Therefore, equation 2.1 is used for both models despite the determination of the fluence rate at each triangular face.

The photons that reach the surface of the cavity can interact with the tissue in different ways, see figure 2.3. They can be absorbed by the tissue and ensure interaction with the PS that is present, they can directly be reflected back into the cavity or they will scatter through the tissue and eventually reach the surface again and re-emit back into the cavity. To what extent these interactions take place depends on the tissue that

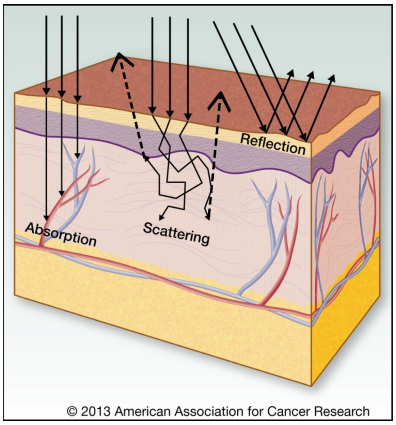

Figure 2.3: Interactions of the photon with the tissue: absorption, scattering, reflection [34].

is illuminated and the characteristics of the light, such as the wavelength. For the red light that is used during cPDT, scattering dominates reflection and absorption. The scatter (μ_s) and absorption (μ_a) coefficient give the probability that respectively scatter and absorption take place per unit distance. In a cavity, no light can escape, so the build-up of light fluence at the tissue will be higher than for example in the skin [35].

2.3 | Analytical model

The analytical light distribution model can be used to estimate the light distribution in the nasal cavity using a spherical bulb diffuser. The analytical model simulates the fluence rate that will be measured at each face of the triangular mesh. The fluence rate in the nasal cavity can be measured by holding an isotropic measure probe just above the surface of the nasal cavity, see figure 2.4. The fluence rate that will be measured contains the incident fluence rate, the scattered fluence rate from surrounding faces and the back-scattered fluence rate from the face itself, see equation 2.2. The pseudocode for the analytical light distribution model is shown in algorithm 1.

$$\phi_{measured} = \phi_{inc} + \phi_{scatter} + \phi_{backscatter} \tag{2.2}$$

Where $\phi_{measured}$ is the fluence rate (mW/mm^2) measured with the isotropic measure probe at one face, ϕ_{inc} is the fluence rate contribution of the incident light (mW/mm^2), $\phi_{scatter}$ is the fluence rate contribution of the scattered light from other faces (mW/mm^2) and $\phi_{backscatter}$ is the fluence rate contribution of the back scattered light from the face itself (mW/mm^2).

Algorithm 1 Analytical light distribution model

Require: $SL, S, Cavity, O, vertices, R_d, cos(\theta_1), cos(\theta_2), n, A_1$
Ensure: $\phi_{measured}$

Step 1: Calculate ϕ_{inc} in two steps:

A) Calculate shaded faces with ray-casting:

$L \Leftarrow linspace(SL, O)$
$C \Leftarrow Cavity(L)$
if C contains 1 **then**
    $f_{inc} \Leftarrow 1$
else
    $f_{inc} \Leftarrow 0$
end if

B) Calculate ϕ_{inc}:

$r \Leftarrow \sqrt{(SL - O)^2}$
$\phi_{inc} \Leftarrow \frac{S f_{inc}}{4\pi r^2}$

Step 2: Calculate $\phi_{scatter}$ in three steps:

A) Calculate shaded faces with ray-casting:

for Each receiving face **do**
    for Each vertex of the reflecting faces **do**
        $L_r \Leftarrow linspace(Vertices, O)$
        $C_r \Leftarrow Cavity(L_r)$
        if C_r contains 1 **then**
            $f_{reflect} \Leftarrow 1$
        else
            $f_{reflect} \Leftarrow 0$
        end if
    end for
end for

B) Calculate distance from receiving face to all other reflecting faces:

$magn \Leftarrow \sqrt{(O[x] - O[x])^2 + (O[y] - O[y])^2 + (O[z] - O[z])^2}$

C) Calculate the contribution of fluence rate at all faces due to scattering:

$E[0] \Leftarrow \phi_{inc}$
for i=n **do**
$\phi_{received} \Leftarrow \frac{E[i]R_d cos(\theta_1)cos(\theta_2)A_1 f_{reflect}}{\pi magn^2}$ $E[i+1] \Leftarrow \phi_{received}$
end for

Step 3: Calculate $\phi_{backscatter}$:

$\phi_{backscatter} \Leftarrow sum(E)R_d$

Step 4: Calculate $\phi_{measured}$, the total fluence rate that each face receives due to incident light, reflected light and back-scattered light:

$\phi_{measured} \Leftarrow E + \phi_{backscatter}$

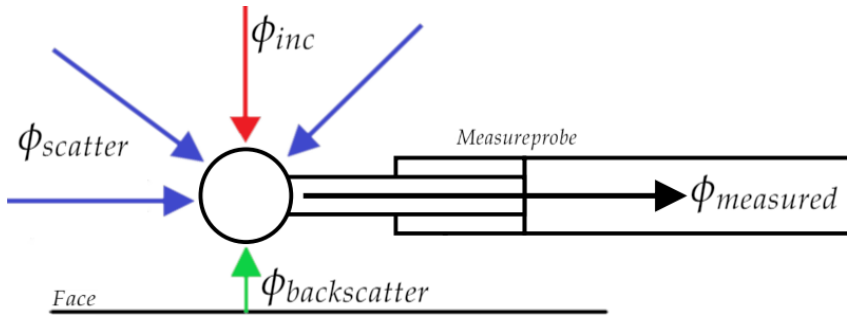

Figure 2.4: The total fluence rate that is measured with the probe, consisting of the incident fluence rate (red), scattered fluence rate (blue) and back-scattered fluence rate (green).

The first term of equation 2.2, the incident fluence rate, can be calculated with a small adjustment to equation 2.1. This equation describes the incident fluence rate using the distance from the light source to the origin of the face and the output power of the light source. However, it is not known if the incident light reaches the face, in other words if the face is located in a shaded area or not. A face is located in a shaded area if the light beam is blocked by another face. To determine if another face blocks the incident light beam, three lines are created from the light source to each vertex of the face. If the line crosses a non aerial voxel, the vertex lays in a shadowed area. The fraction (f) of the face that receives incident light will be determined using these lines. If all vertices are in a shadowed area, f will be zero, if one vertices receives incident light, f will be $1/3$ and so on. In the analytical model, the incident fluence rate will be calculated using equation 2.3.

$$\phi_{inc} = \frac{S f_{inc}}{4\pi r^2} \tag{2.3}$$

Where ϕ_{inc} is the fluence rate (mW/mm^2) on the face due to the incident light, S is the output power of the spherical bulb diffuser (mW), f_{inc} is the fraction of the face that receives incident light and r is the distance from the spherical bulb diffuser to the origin of the face (mm).

The contribution of the scattered fluence rate ($\phi_{scatter}$) depends on the amount of light that is reflected by the tissue. The analytical model assumes that the surface of the nasal cavity can be described as a Lambertian surface. A Lambertian surface re-emits photons diffusely. The intensity of the reflected light is dependent on the cosine of the angle (ω) between the incidence light beam and the normal of the surface, see figure 2.5. Furthermore, the ratio of the incoming light that is being reflected at the face, the diffuse reflection coefficient (R_d), is of importance to determine the amount of light reflected back into the cavity. The distribution of the reflected light at a surface can be described by the Lambert's cosine law, see equation 2.4.

$$I(\theta) = E R_d cos(\omega) A \tag{2.4}$$

Where I is the fluence rate (mW/mm^2) reflected at the angle between the normal of the face and the outgoing beam (ω), E is the incident fluence rate received by the face (mW/mm^2), R_d is the diffuse reflection coefficient and A is the surface area (mm^2) of the Lambertian patch.

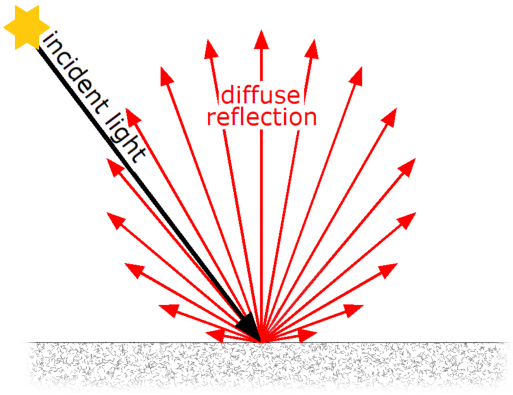

Figure 2.5: The incident term and the scatter term of the light distribution shown schematically [36].

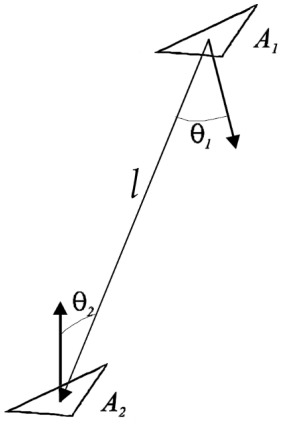

Figure 2.6: Schematic representation of the receiving face (A_1) and the reflecting face (A_2) [37].

A face receives reflected light from another face (the reflecting face), see figure 2.6. The amount of light that is received by a face from a reflecting face can be calculated with equation 2.5.

$$\phi_{received} = \frac{\phi_{Ana,inc} R_d cos(\theta_1) cos(\theta_2) A_1 f_{reflect}}{\pi l^2} \tag{2.5}$$

Where $\phi_{received}$ is the fluence rate (mW/mm^2) that the face will receive from the reflecting face, θ_1 is the angle between the normal vector of the reflecting face and the reflected light beam, θ_2 is the angle of incidence, $A_{1,k}$ is the surface area of the receiving face (mm^2), $f_{reflect}$ is the fraction of the receiving face that is not located in a shaded area and l is the distance between the emitting face and the receiving face (mm).

Reflection does not only take place once, but it will take on till all the light is absorbed in the tissue. The number of reflections that will take place till all the light is absorbed is dependent on R_d. In the analytical model it is assumed that all the light is

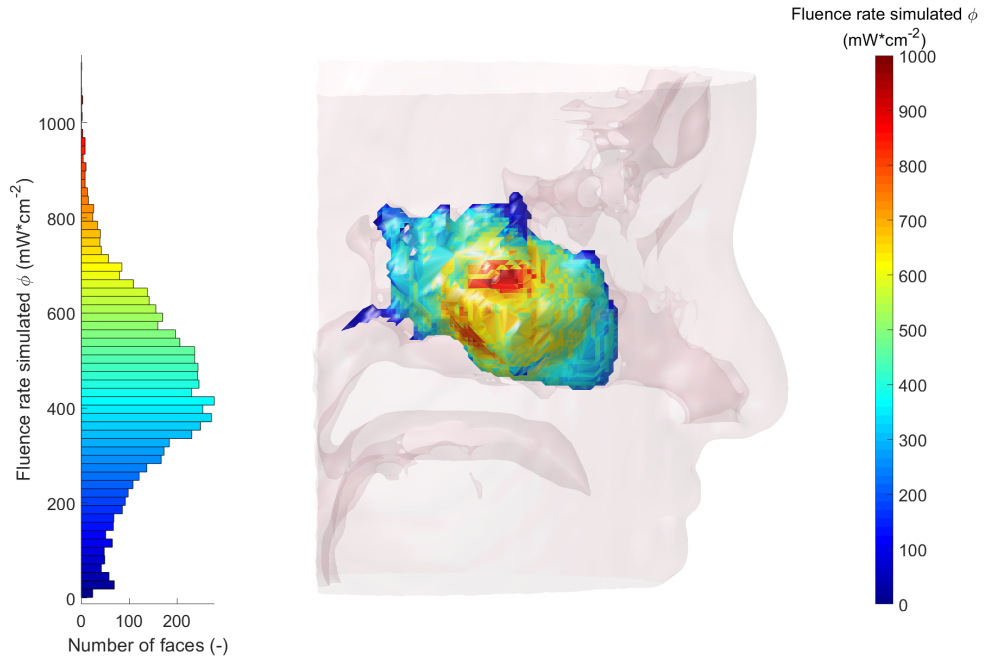

Figure 2.7: An example of the light distribution calculated with the analytical model using a spherical bulb diffuser with an output power of 1000 mW. The histogram (left) shows the amount of faces that receive a certain amount of fluence rate. In the middle, the light distribution is shown in a 3D mesh of a para-nasal cavity with the colour bar on the right.

absorbed when less than 1% of the light that is emitted by the light source is left in the cavity (in case of an R_d of 0.81, 22 reflections are simulated: $S0.81^{22} = S0.0097$). The total contribution of the scattered fluence rate on a face can be described with equation 2.6

$$\phi_{scatter} = \sum_{j=1}^{n} \sum_{k=1}^{m} \phi_{received_{j,k}} \tag{2.6}$$

Where n is the number of reflections and m is the total amount of surrounding faces.

The back-scattered fluence rate is defined as the total amount of fluence rate on the face that is reflected back into the cavity. This is dependent on R_d, ϕ_{inc} and $\phi_{received}$, see equation 2.7.

$$\phi_{backscatter} = R_d(\phi_{inc} + \phi_{received}) \tag{2.7}$$

An example of the light distribution in a cavity calculated with the analytical model using an R_d of 0.81 can be seen in figure 2.7.

2.4 | Empirical model

Another light distribution model was created next to the analytical model. The aim of the empirical model is to simulate the light distribution with simple calculations resulting in a shorter calculation time. The pseudocode for the empirical light distribution model is shown in algorithm 2. This empirical model is based on the basic equation 2.1 and a factor that describes the build-up (β) due to reflection and scattering of the light. The ratio between ϕ_{inc} and $\phi_{measured}$ is the β factor, see equation 2.8.

$$\beta = \frac{\phi_{measured}}{\phi_{inc}} \tag{2.8}$$

The β factor is dependent on the distance between the light source and the surface. During measurements, a linear relation was found between the build-up factor and the distance, see equation 2.9 [31, 32]. The slope of the build-up function depends on the characteristics of the tissue and will be different per patient.

Algorithm 2 Empirical light distribution model

Require: $SL, S, O, \beta(r)$
Ensure: $\phi_{spherical}$

$r \Leftarrow \sqrt{(O - SL)^2}$
$\phi_{spherical} \Leftarrow \frac{\beta(r)S}{4\pi r^2}$

$$\beta(r) = 0.13r + 1 \tag{2.9}$$

Where r is the distance from the light source to the surface (mm). The slope of 0.13 in this build-up function is based on measurements using porcine tissue.

The empirical model is able to simulate the light distribution in the sino-nasal cavity using one single equation, see equation 2.10. This equation is a combination of the incident light term and the build-up function, respectively equation 2.1 and 2.9. An example of the light distribution in a cavity calculated with the empirical model can be seen in figure 2.8.

$$\phi_{spherical} = \frac{S(0.13r + 1)}{4\pi r^2} \tag{2.10}$$

Where $\phi_{spherical}$ is the fluence rate in (mW/mm^2), S is the output power of the spherical bulb diffuser and r is the distance between the spherical bulb diffuser and the surface (mm).

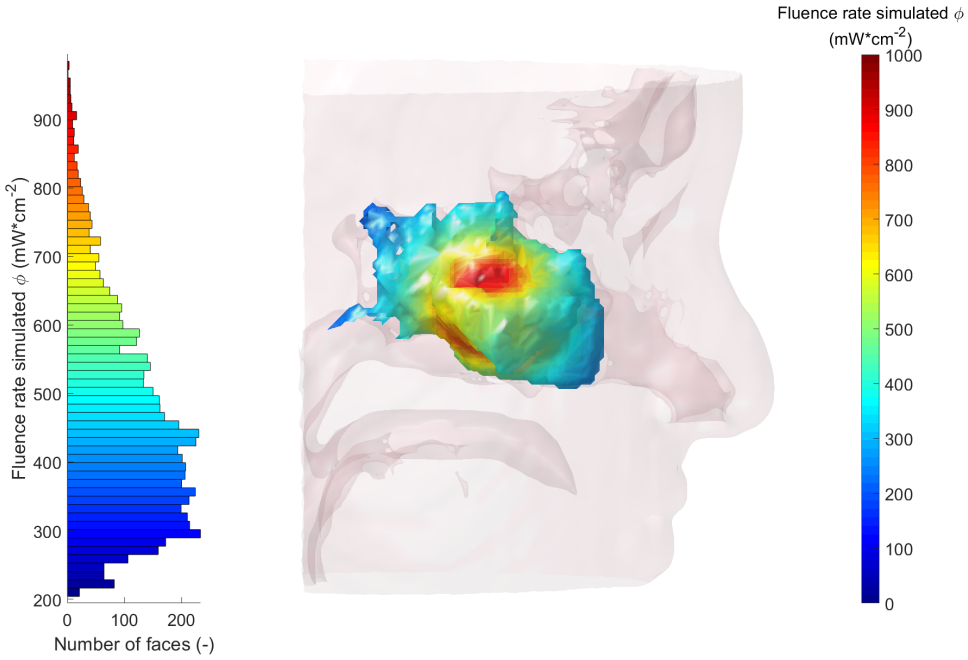

Figure 2.8: An example of the light distribution calculated with the empirical model using a spherical bulb diffuser with an output power of 1000 mW. The histogram (left) shows the amount of faces that receive a certain amount of fluence rate. In the middle, the light distribution is shown in a 3D mesh of a para-nasal cavity with the colour bar on the right.

2.5 | Comparing both models

Both models, the analytical and empirical, are able to predict the light distribution in the sino-nasal cavity given the CT scan of the patient, the location and the output power of the spherical bulb diffuser. The analytical model also needs the R_d value to accurately determine the amount of reflections that take place and the empirical model needs the β value to take the contribution due to reflections into account. Previous research has shown that both models are accurate in the prediction of the light distribution, especially when the tissue has a high absorption coefficient (μ_a). This accuracy of both models is tested on 3D printed phantoms of the sino-nasal cavity of three patients and on one porcine tissue phantom. The root mean square of the analytical model for phantom measurements was 20.8 and for the empirical model 27.5 [32]. The light distibution in a sino-nasal cavity calculated with the empirical and analytical model are not exactly the same. The difference between both models at each location in the sino-nasal cavity

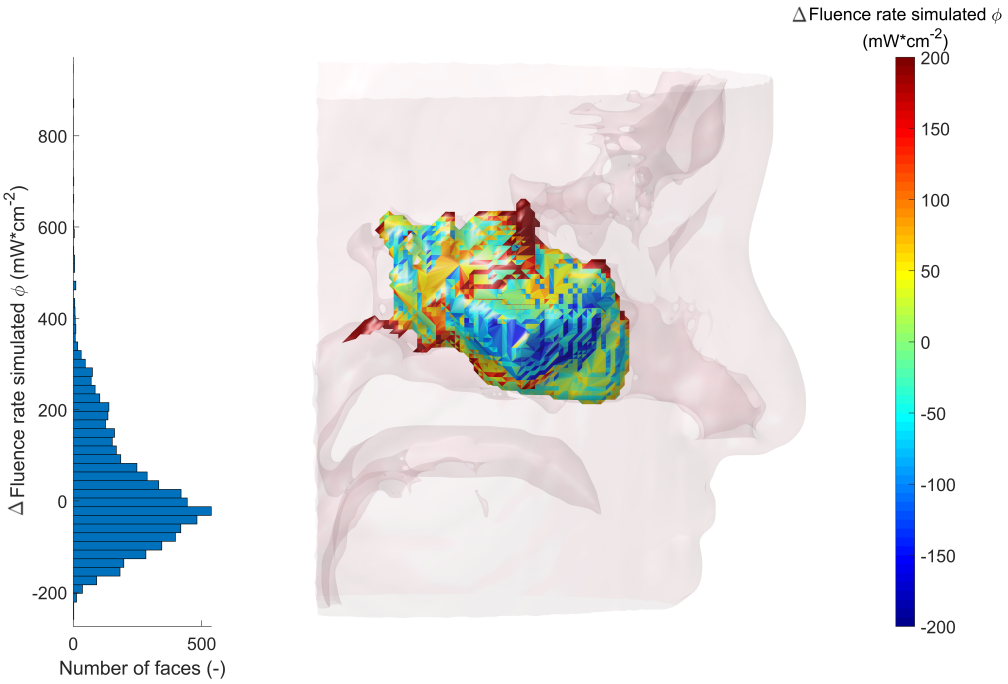

Figure 2.9: The light distribution in the sino-nasal cavity is calculated with the empirical and the analytical model. The difference between both distributions is shown in this figure (empirical minus analytical). The histogram (left) shows the number of faces per difference in fluence rate between both models. In the middle, the difference of the light distribution is shown in a 3D mesh of a para-nasal cavity with the colour bar on the right.

can be seen in figure 2.9. The analytical model is subtracted from the empirical model. A positive fluence rate difference means that the empirical model calculated a higher fluence rate at a certain face than the analytical model. The empirical model shows higher fluence rates at faces that do not receive incident light, due to the inability to calculate which face is located in a shaded area.

An important difference between both models is that the analytical model is able to take shaded areas into account. In the current implementation, this is not possible for the empirical model. The empirical model only uses the distances between the light source and the centre of each face, a linear equation is used to calculate the fluence rate on this specific face. The analytical model first uses a ray-tracing algorithm to determine if the specific face is located in a shaded area or not, then the fluence rate is calculated for every reflection till only 1% of the initial light dose is present in the cavity. During each reflection, the shaded areas are again taken into account. The faces that do not receive initial light can receive some light due to reflection.

The analytical model is more complex than the empirical model resulting in a big difference in calculation time between both models. The analytical model was able to calculate the light distribution in a sino-nasal cavity in about 15.9 seconds, while the empirical models takes only 8.10^{-5} seconds for the same cavity. The empirical model only calculates the distances from the light source to each face, the calculation time is proportional to the amount of faces. The analytical model is more complex due to the calculation of shaded areas, but also due to the calculation of multiple reflections. The analytical model calculates the distance from light source to each face and the distances from each face to all surrounding faces. Due to this difference in calculation time it is easier to implement the empirical model into a cPDT planning tool for the automatic optimisation of the optimal source location. The analytic model could be used for verification of the overall result.

3 Evaluation of the build-up function

3.1 | Introduction

The analytical and empirical models are both able to estimate the light distribution in the sino-nasal cavity during cPDT. The empirical model can calculate this light distribution with one single equation. This equation consists of the incident fluence rate and the contribution of scattering, see equation 2.10. The contribution of scattering can be determined with the build-up function which gives the relation between the β factor and the distance from the light source to the surface of the cavity (r).

Earlier research suggested a linear relation between the distance r and the β factor, $ar + 1$ [31, 32]. The slope of this function (a) differs for each patient, because it is dependent on the geometry of the cavity and on the R_d of the tissue. However, it is questionable if the build-up function is correctly described as a linear function. If this build-up function is not correct, the empirical model does not describe the light distribution in the cavity adequate.

Furthermore, it is important to know if there is a relation between the build-up function and characteristics of the cavity, such as the surface area and/or the volume and optical properties. If there is a relation between these, it can be used to determine the build-up function for each patient solely using the CT scan. Currently, the empirical model can only be used if the build-up function is determined with dosimetry measurements in the nasal cavity of the patient. It would be easier to implement the empirical model in the clinic if these measurement do not have to take place.

The main aim of this research is to improve the empirical model and to make it accurate. This main aim is reached by answering two sub questions. The first sub question is whether the β factor can be described with a linear function as stated in previous research. The second sub question is if there is a relation between the characteristics of the cavity and the build-up function and how this relation can be described. Both sub questions are answered by calculating the β factor for spheres with different radii and with varying R_d and r values.

3.2 | Method

3.2.1 | Empirical model

The empirical model describes the light distribution in a triangular mesh of a sino-nasal cavity given the source location and its output power. This model uses only one simple equation to calculate the light distribution, see equation 3.1. The hypothesis was that the build-up function ($\beta(r_k)$) could be described as $ar + 1$.

$$\phi_{predicted} = \beta(r_k)\frac{S}{4\pi r_k^2} \tag{3.1}$$

Where $\phi_{predicted}$ is the fluence rate at the k^{th} face, $\beta(r_k)$ is the build-up function, S is the output power of the light source, r_k is the distance between the light source and the k^{th} face.

3.2.2 | Relation β factor and r

The build-up function gives the relation between the β factor and the distance from the light source to the surface of the cavity r. To determine how this relation can be described, the β factor should be calculated for different values of r. The β factor can be calculated using equation 2.8 and is in this research determined using the analytical model using an output power of the light source of 1000 mW. The incident fluence rate (ϕ_{inc}) and the measured fluence rate ($\phi_{measured}$) can be calculated with this model taking the reflections of light inside the cavity into account.

The relation between the β factor and r is found by plotting the β factor against the distance r. Subsequently, a trend line is composed that describes the relation between the β factor and r. The root mean squared error (RMSE) is calculated to determine the quality of the trend line, see equation 3.2. The lower RMSE, the better the fit of the trend line. The trend line that describes the available data the best is the build-up function. The composed trend line is compared with the linear trend line using the RMSE.

$$RMSE = \sqrt{\frac{\sum_{t=1}^{T}(\hat{y}_t - y_t)^2}{T}} \tag{3.2}$$

Where RMSE is the root mean squared error, $\hat{y}_t$ is the calculated β factor, y_t is the estimated β factor using the trend line, T is the total number of calculated β factors and t is the counter which indicates which β factor is taken.

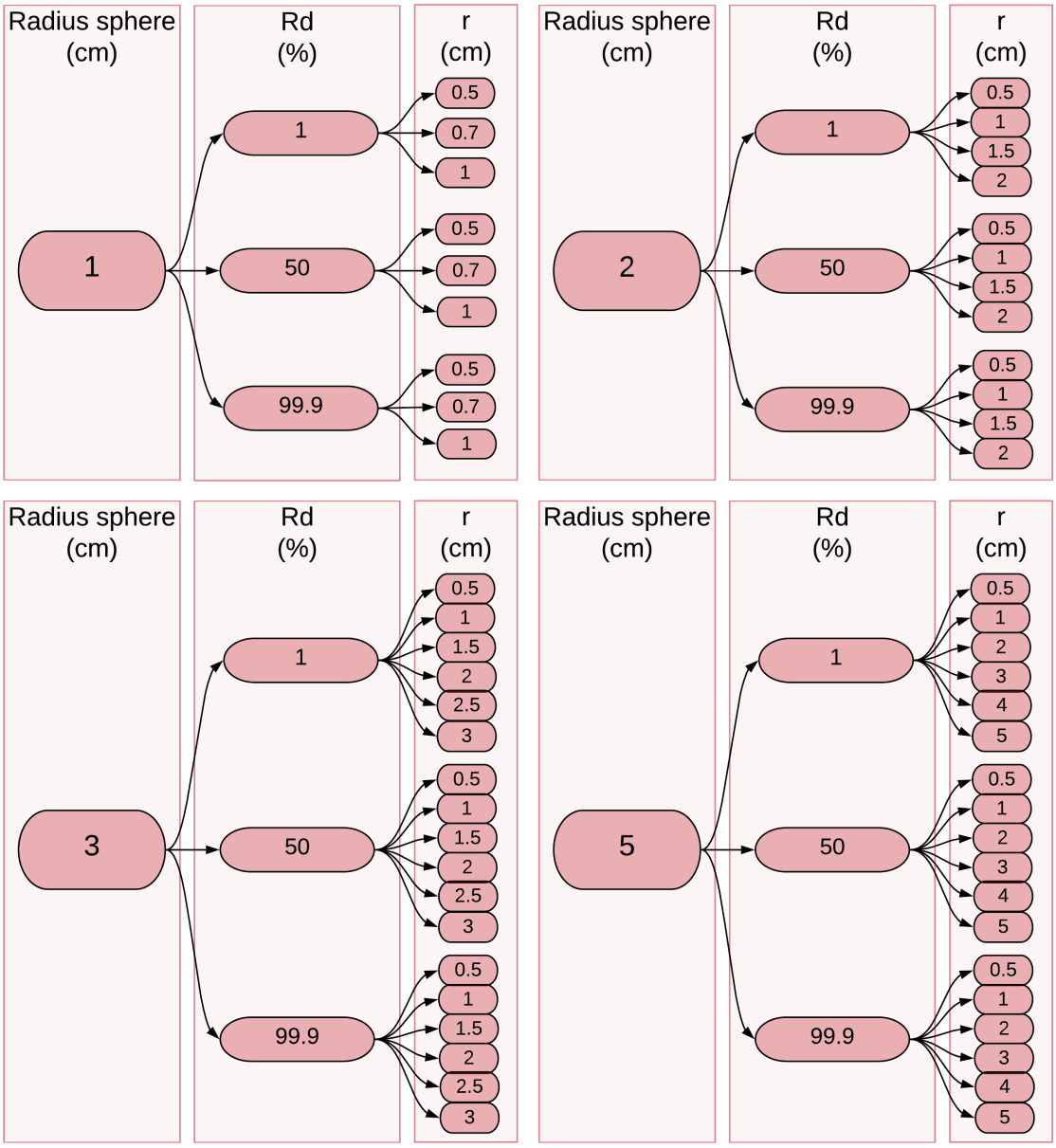

Figure 3.1: Summation of all variables used in this research. For example, the β factor is calculated for a sphere with radius of 1 cm and R_d of 1% at r equal to 0.5, 0.7 and 1 cm.

3.2.3 | Relation build-up function and characteristics of cavity

To determine the relation between the build-up function and the size of the cavity, the β factor is calculated for spheres with different radii (one, two, three and five centimetre). The build-up functions for these different spheres are compared with each other by looking at the volume, surface area and the ratio between these (volume/surface area).

The R_d of the tissue has influence on the build-up function. The R_d is tissue dependent and defines how much of the light is reflected back into the cavity. If the R_d of a tissue is equal to 100%, all photons reaching the tissue will be reflected back into the cavity. In this research, three different values of R_d: 1%, 50% and 99,9%, are used to see how the build-up function behaves with a different R_d. It is expected that the β factor will be higher using a higher R_d.

Concluding, the β factor is calculated for four different spheres, three different R_d values and with the light source at different distances from the surface of the cavity, see figure 3.1.

3.3 | Results

First, the relation between the β factor and the distance from the light source to the surface (r) is assessed. The light distributions in a sphere with radius of 3 cm for different locations of the light source are shown in figure 3.2. In this research, a quadratic relation between these two is found following the standard quadratic formula $cr^2 + d$ in which c is the coefficient of the quadratic term (from now on referred to as coefficient) and d

Table 3.1: RMSE for a linear and quadratic trend line using different radii and R_d values. The lowest RMSE value per setting is indicated in green.

Sphere radius	R_d	RMSE Linear	RMSE Quadratic
1 cm	1%	0,0003	0,0004
	50%	0,0379	0,0243
	99,9%	0,3893	0,1579
2 cm	1%	0,0007	0,0003
	50%	0,0731	0,0203
	99,9%	0,6400	0,1453
3 cm	1%	0,0007	0,0003
	50%	0,0774	0,0203
	99,9%	0,7247	0,1453
5 cm	1%	0,0008	0,0002
	50%	0,0933	0,0228
	99,9%	0,9894	0,0893

is the y-intercept. The calculated β factor at different r values and its quadratic relation using a sphere with radius 3 cm is shown in figure 3.3A. Table 3.1 shows the RMSE values of all trend lines calculated for the quadratic relation and for a linear relation. The lowest RMSE value is also indicated in this table. What stands out is that the RMSE for a quadratic relation is almost always lower than that for a linear relation, except for a sphere radius of 1 cm and an R_d of 1%. In this case, the RMSE for a linear equation is a bit lower than for a quadratic equation. Furthermore, the RMSE is always lower for an R_d of 1% than for 50% and 99.9%.

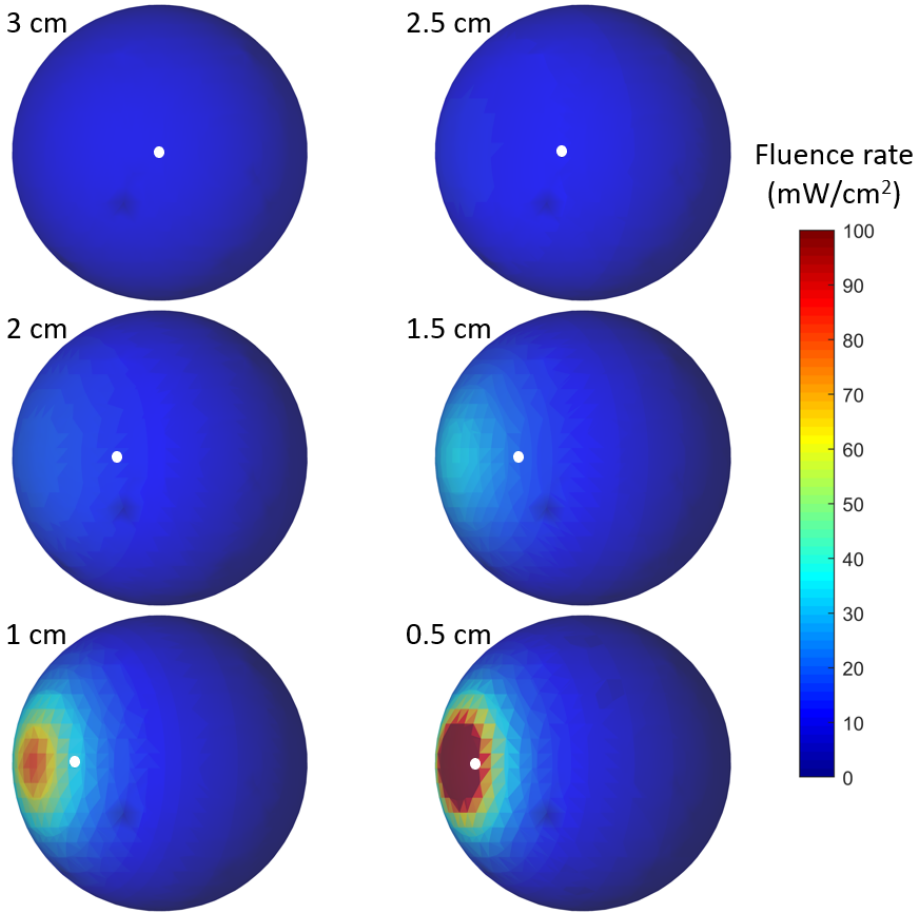

Figure 3.2: Light distribution in a sphere with radius of 3 cm calculated with the analytical model with an Rd of 1% and S of 1000 mW. The location of the spherical bulb diffuser is varied and the smallest distance between the light source and the wall is indicated.

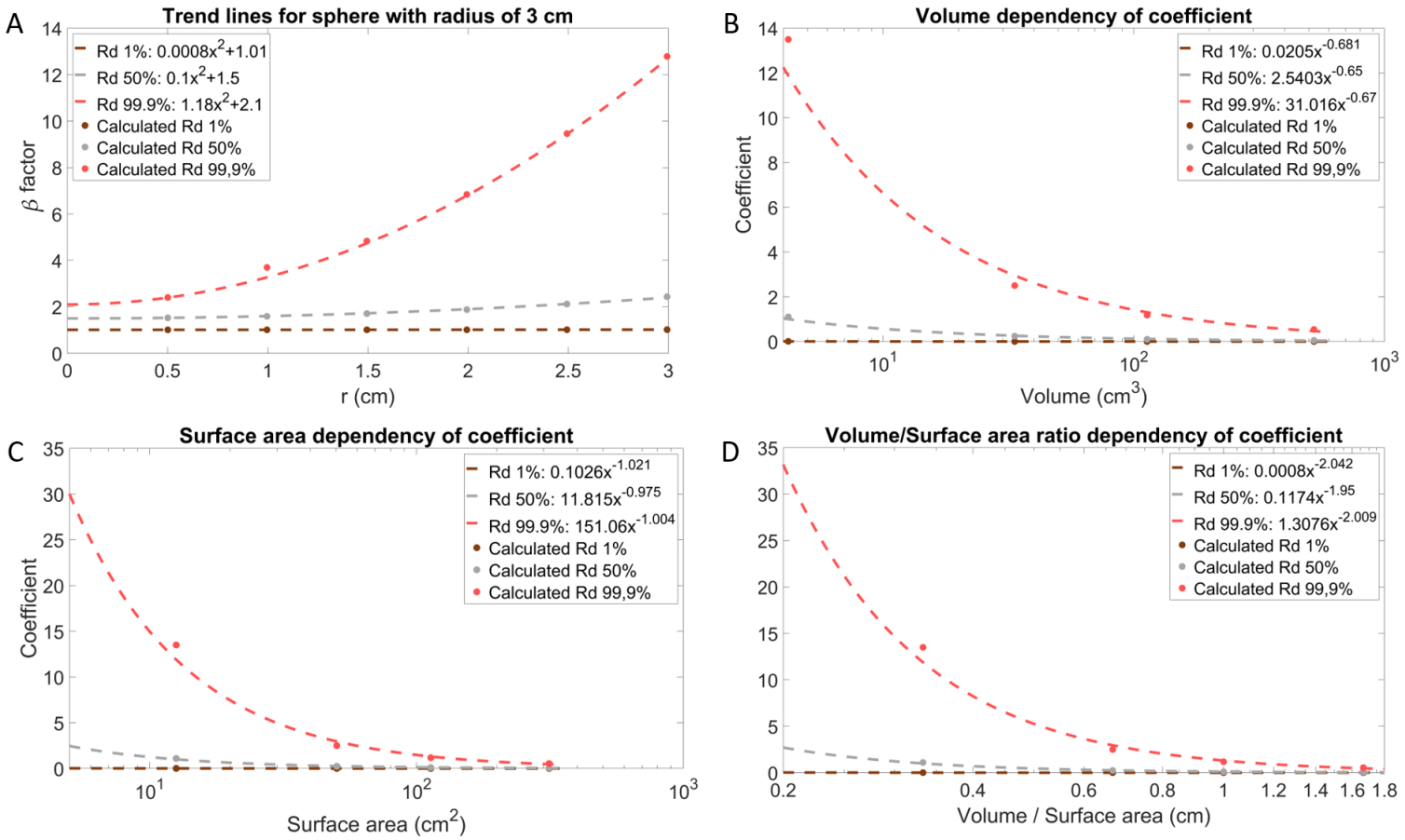

Figure 3.3: A: Plot of the trend lines showing the relation between the β factor and the distance r for different R_d values using a sphere with radius of 3 cm. B: Volume dependency of coefficient of the build-up function. C: Surface area dependency of coefficient of the build-up function. D: Ratio between volume and surface area dependency of coefficient of the build-up function. The power function for each line is displayed in each graph in which the x refers to the variable on the x-axis of that graph.

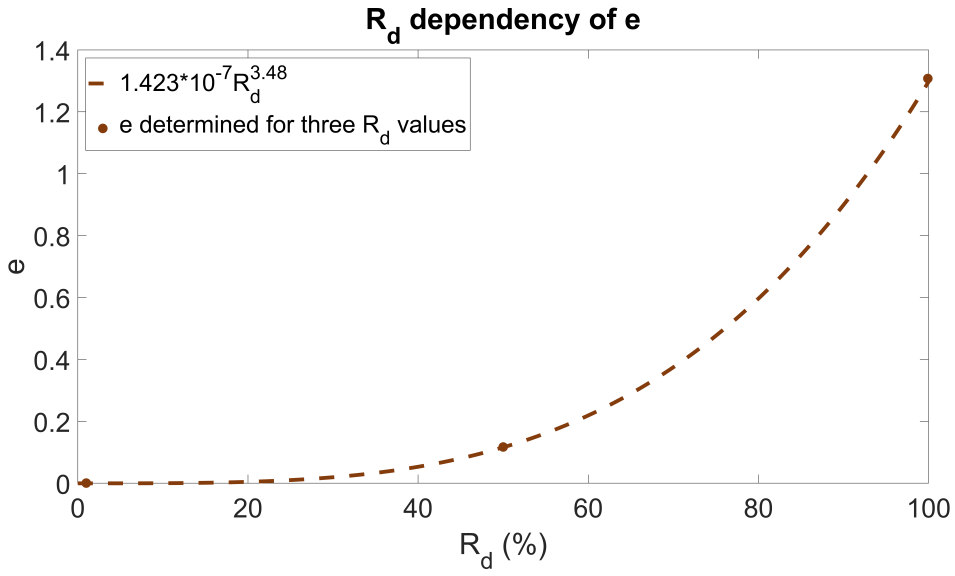

Figure 3.4: Relation between R_d and e of the power function that describes the ratio (volume/surface area) dependency of the coefficient of the build-up function. The three determined e values are plotted in this graph and the corresponding trend line is given.

By comparing the quadratic equations of different settings with each other, it stands out that the coefficient of the quadratic function is dependent on the sphere radius and R_d. This dependency is assessed by finding the relation between the coefficient and the volume and surface area of the cavity and the ratio between both. In figure 3.3B, C and D, the volume, surface area and the ratio between both is plotted against the coefficient of the quadratic function. The corresponding power function in the form ex^f is also displayed in these plots. The f of the power function is almost the same for each group, namely -0.65 for the volume dependency, -1 for the surface area dependency and -2 for the ratio dependency. The e in each trend line differs from each other when another R_d value is used. This dependency is also evaluated, the R_d values are plotted against e to look for the relation between both, see figure 3.4. This is only performed for the power functions of the ratio between the volume and surface area. The relation between R_d and e can be described with the function: $1.423.10^{-7}R_d^{3.48}$.

By looking at the build-up functions that can be described as a quadratic equation there is another thing that stands out. The y-intercept is highly dependent on R_d. Comparing the build-up functions, d is constant with a constant R_d. With an R_d of 1%, 50% and 99.9%, d is respectively 1.01, 1.5 and 2.1. The relation between the y-intercept and R_d can be described with the linear function: $0.011R_d + 0.9821$, see figure 3.5. This function can be simplified to the equation: $1 + R_d$, where R_d is converted to a range between 0 and 1.

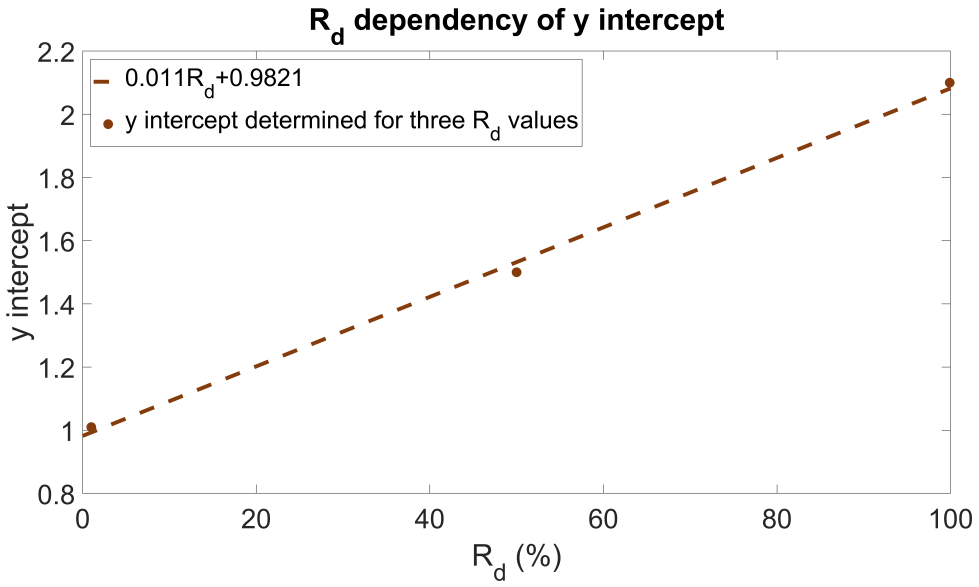

Figure 3.5: Relation between R_d and y-intercept of the build-up function. The y-intercept is the same for each size of the cavity. The three calculated y-intercept points are plotted in this graph.

The whole build-up function can be described with one equation which depends on the ratio of the volume and surface area of the cavity and R_d. The build-up function can be described as shown in equation 3.3.

$$\beta(r_k) = 1.423.10^{-7} R_d^{3.48} (\frac{V}{A})^{-2} r_k^2 + (\frac{R_d}{100} + 1) \tag{3.3}$$

Where $\beta(r_k)$ is the build-up function, R_d is the reflection coefficient in percentage, V is the volume of the cavity in cm^3, A is the surface area of the cavity in cm^2, r is the distance from the light source to the k^{th} face in cm.

3.4 | Discussion

The main goal of this research was to optimise the quality of the empirical light distribution model. The first sub-goal was to determine if the build-up function can be described with a linear function as stated in previous research, or that this relation is not fully correct. The β factor is calculated for four spheres with a varying radius, for different R_d values and different values of r using the analytical model.

By plotting the β factor for different values of r, the build-up function could be determined. The β factor is higher for higher values of r. With a higher value of r, the

incident fluence rate will be lower than with a lower value of r, see equation 2.1. Furthermore, the higher r, the higher the contribution of scattering from the surrounding faces. The photons need to travel over a larger distance to reach the surrounding faces from the light source and travel back to the measured face when r is lower. This results in a lower contribution of scatter for lower values of r. The results show that the relation between the β factor and the distance from the light source to the surface (r) can be described the best using a quadratic function of the form $cr^2 + d$. The RMSE value of the quadratic function is lower than that for the linear function for all except one. It can thus be suggested that the build-up function should be described as a quadratic function and not as a linear function.

The second sub-goal was to find out if there is a relation between characteristics of the cavity and the build-up function. This is done by evaluating the coefficient and the y-intercept of the build-up function. The results show that the coefficient of the build-up function is dependent on the size of the sphere and R_d. When R_d is higher, more scattering and back-scattering of the photons will take place (less absorption of photons in the tissue). This results in a higher $\phi_{measured}$ relative to a lower R_d and therefore a higher β value. The geometry of the cavity (ratio of the volume and surface area) does also influence the β factor. A higher volume to surface area ratio (decreasing surface irregularity) results in a lower β factor. The relation between the coefficient and the volume and surface area of the cavity and the ratio of both can be described with a power function which is dependent on R_d. The relation of the power function and R_d using the ratio of the volume and surface area is also determined. The ratio between the volume and surface area is used for this analysis, because this ratio gives more information about the shape of the cavity. A lower ratio is associated with an increasing surface irregularity. Using all these relations, the coefficient of the build-up function can be describe using the ratio between the volume and surface area and R_d.

The y-intercept of the build-up function only depends on R_d. This relation can be described with the linear function $0.011R_d + 0.9821$. This relation can be simplified with the formula: $R_d + 1$, where R_d is normalised to a range of 0 to 1. The y-intercept indicates what the R_d of the tissue is. When r is equal to zero, the incident light term is very high, because it does not decrease with $1/r^2$. The back-scattered term is equal to the incident light term times R_d and the amount of scattering from the surrounding faces is very low. Resulting in the equation for the β factor of: $\beta = \frac{\phi_{inc} R_d}{\phi_{inc}}$.

In this research, the build-up function is described depending on R_d and the size of the cavity, see equation 3.3. In this equation, the simplified function for the determination of y-intercept can be used. However, a drawback of this study is the amount of simulations that are performed. The relations defined in this research should be verified using more values of R_d.

Ideally, the build-up function can be defined by only using the characteristics of the

cavity, such as the volume or surface area. Because these characteristics can be determined using the CT scan of the patient. However, the results of this research show that the build-up function also depends on R_d. Therefore, R_d should be determined for each patient prior to the cPDT planning. Currently, research is performed to determine if the R_d is about the same for every sino-nasal cavity. When this is the case, the determination of the build-up function can be performed solely using the CT scan. If this is not possible, the R_d should be measured in the patient's sino-nasal cavity. If this is the case, it would be easier to determine the build-up function right away with the measurements in the cavity. This could be done with an instrument that still has to be developed. A light source should be placed inside the sino-nasal cavity with multiple isotropic measuring probes connected to it on a known distance. This way, the build-up function can be determined and the relations between the build-up function and the characteristics of the cavity, found in this research, are not needed anymore.

This research describes that the build-up function is dependent on the geometry of the cavity and R_d and this relation is described. However, this relation is based on the use of a spherical cavity. It is possible that this relation is different in a less spherical cavity, such as the sino-nasal cavity. When the cavity has more niches, it is expected that the β factor will be generally lower due to the amount of shaded areas. It is conceivable that the relation between the build-up function and the size of the cavity and R_d is different when it is determined using a sino-nasal cavity instead of a sphere.

Another limitation of this research is that the β factor is calculated with the analytical model and not using real measurements. It is possible that the analytical model does not represent the reality fully and that the calculated β factor is not exactly correct. Therefore, a recommendation for further research would be to perform the β factor measurements using a sphere with a predefined size and sino-nasal cavities with a known R_d value. These measurements should be used to compare the measured β factor with the calculated β factor to validate the analytical model and the build-up function that is found during this research.

To be able to use the size of the cavity and R_d in the determination of the build-up function, more measurements should be performed using different shapes and sizes of the cavity and by varying R_d values. This way, the relation between the coefficient and y-intercept and the size and R_d of the cavity can be determined with certainty.

3.5 | Conclusion

In conclusion, the build-up function can be described as a quadratic function $cr^2 + d$. The coefficient of the quadratic function depends on the R_d and size of the cavity. The relation between the coefficient and the volume, surface area and a ratio between both can be described with a power function. The y-intercept of the build-up function de-

pends on R_d and can be described with the linear function $0.011R_d + 0.9821$. This linear function can possibly be simplified to $R_d + 1$ when R_d is normalised to a range between 0 and 1. Combining all relations, the build-up function can be described with the equation:

$$\beta(r_k) = 1.423.10^{-7} R_d^{3.48} (\tfrac{V}{A})^{-2} r_k^2 + \tfrac{R_d}{100} + 1$$

These relations can be used to determine a patient specific build-up function when the geometry of the cavity and R_d are known. However, more research should be done using more variations of R_d and more realistic cavity shapes to confirm the results presented in this research. Furthermore, research should be performed to determine if a standard R_d value can be used for each sino-nasal cavity.

4 Development of a cPDT planning tool

4.1 | Introduction

Photodynamic therapy (PDT) is used to treat superficial tumours in the head and neck region and is proved to be effective [22, 38–40]. However, the patients experience some side effects after treatment with PDT, such as skin burning and extreme pain. To date, several studies have focused on increasing the effectiveness of the PDT treatment and lowering the side effects. Some studies are aiming to develop tumour specific photosensitizers that only accumulate in the tumour tissue and not in the healthy tissue, leading to a decrease of the side effects [19, 41, 42]. Other studies are mainly focused on increasing the effectiveness of the PDT treatment by ensuring a sufficient light distribution on the tumour tissue. Betrouni et al. [43], Sandell et al. [44] and Zhu et al. [45, 46] have all tried to create a real time light dosimetry model for intrapleural PDT. Several other studies are focused on the development of treatment planning systems for interstitial PDT [47–51].

Up till now, no studies have developed a planning system for the treatment of sino-nasal carcinomas with cavity PDT (cPDT). The dosimetry calculations in the sino-nasal cavity is very difficult due to the complex geometry of these cavities and intra and inter patient variations in optical properties. Two light distribution models are already developed at the Netherlands Cancer Institute in Amsterdam [31, 32]. These models are able to calculate the light distribution in the nasal- and paranasal sinuses if the location of a spherical bulb diffuser is given together with its output power and the CT scan of a patient. These models can be used to create a planning tool that is able to determine the optimal light source location (OSL) with its optimal output power ensuring a sufficient fluence rate on the tumour tissue.

The goal of this research is to develop a cPDT planning tool that is able to calculate the OSL and the output power using the CT scan of the patient. The search for the OSL and its output power can be described as an optimisation problem and can be solved with mathematical optimisation. Mathematical optimisation can be performed using different methods. Which method should be used is fully dependent on the optimisa-

tion problem. The cPDT planning tool is based on this optimisation method. To create this cPDT planning tool, multiple substeps have to be taken. The first sub-goal is to determine how the problem, finding the best source location and output power for an effective treatment of cPDT, can be described mathematically. This mathematical description of the problem is called an objective function or cost function. The description of this objective function will be evaluated in the first sub-step. The second sub-step is the determination of which optimisation method is able to tackle the problem most efficiently. Multiple methods are available and each method has its own variables that can be adjusted for a different result of the optimisation. Lastly, the cPDT planning tool will be verified.

The cPDT planning tool developed in this research is based on the empirical light distribution model, which is described in section 2.4. This light distribution model is used because of the short calculation time. The empirical light distribution model is only developed for the use of a spherical bulb diffuser. Being able to handle different types of diffusers is an requirement for the future. The first step to the implementation of the microlens into the empirical model is made in chapter 5. The empirical light distribution model that is used is still based on a linear build-up function and not on the quadratic build-up function which is described in chapter 3.

4.2 | Methodology

4.2.1 | Requirements

There are some requirements that the planning tool and the navigation tool should comply with. These requirements are needed to be able to use the planning tool in the clinic and make it useful for the physician. The main requirements are listed below in random order:

1. Determine OSL and its optimal output power:
   The main goal of the cPDT planning tool is to calculate the source location and its output power which give the best outcomes of the cPDT treatment. This implies that the tumour needs to be illuminated with a sufficient amount of fluence rate. The planning tool should aim that the tumour is illuminated with a fluence rate between the 80 and 120 mW/cm^2. Furthermore, the dose on the healthy tissue should be kept to a minimum to reduce the side effects. So, the goal is to keep the fluence rate on the healthy tissue below 25 mW/cm^2. It is assumed that there is no tissue response with a fluence rate lower than this 25 mW/cm^2. The fluence rate on the tumour tissue is more important than the fluence rate on the healthy

tissue. The OSL should be accurate to 1.5 millimetre, because of the constraint of the used Electromagnetic (EM) navigation system used during cPDT.

2. Multiple locations of the light source:
   Often it is not possible to ensure an illumination of the total tumour tissue using one light source. Therefore, the planning tool should have a possibility to calculate the optimal positions of multiple light sources.

3. Reproducible:
   The planning tool should give the same output every time the script is used to ensure the same quality for each patient.

4. User friendly interface:
   It is important to make a user friendly interface of the planning tool to be able to use the program in the clinic. The physician should be able to use the planning tool without understanding the underlying principles of Python.

5. Implementation in the operation room:
   The cPDT planning tool will give the OSL and its output power. During the cPDT procedure, the physician has to position the light source at exact this OSL. This can be done using an EM navigation system. The planning tool should give the positions of the OSL in CT coordinates, so it is easy to use the EM navigation during surgery.

6. Computational time:
   The OSL and its output power should be calculated within reasonable time. The physician needs to check the results of the optimisation. The planning tool can not be implemented in the clinical workflow if the calculation takes for example the whole day. Therefore, it is important to keep the calculation time below half an hour per patient.

4.2.2 | Planning tool algorithm

The development of the cPDT planning tool can be divided into multiple sub-steps, see figure 4.1. First, a segmentation of the tissue versus air using the CT scan has to be made and the location of the tumour should be delineated inside this segmentation. The second step is the creation of a triangular mesh of the sino-nasal cavity. Subsequently, the system needs to know what the possible locations of the light source inside the cavity are during cPDT, the light source cannot lay too close to the cavity wall. When these three steps have been completed, the fourth step, the optimisation, can be started. When the optimisation gives the OSL and its output power, a visualisation in step five will help with the assessment of the quality of the planning. Last

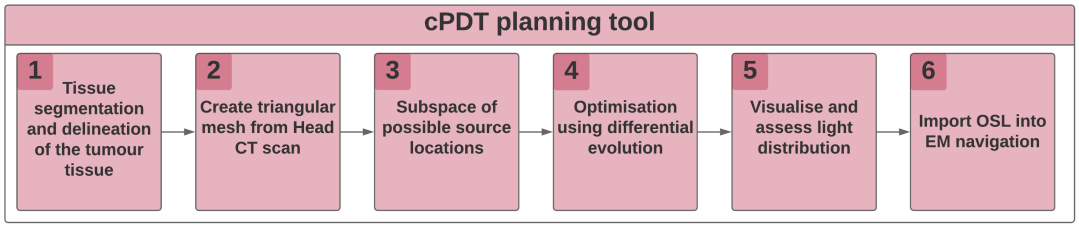

Figure 4.1: Flowchart indicating the six steps that are made with the cPDT planning tool.

but not least, the location of the OSL should be saved so it can be imported into the EM navigation system during the cPDT procedure. Each step will be elaborated below. The cPDT planning tool is programmed in Python using PyCharm Edition 2018.3.5 (JetBrains, www.jetbrains.com/pycharm).

4.2.2.1 | Tissue segmentation and delineation of the tumour tissue

First, a tissue versus air segmentation is made out of the head CT scan using a threshold value of -600 Hounsfield Units (HU). The segmentation is a binary image where tissue is 1 and air is 0. Second, the location of the tumour tissue must be indicated to be able to make a planning that is accurate. The physician has to delineate the tumour/target tissue that has to receive a fluence rate of approximately 100 mW/cm^2 during cPDT. The segmentation and delineation are both performed using the program 3D Slicer 4.10.1 (http://www.slicer.org [52]). The CT scan of the patient is loaded into 3D slicer. The physician is able to draw the tumour/target tissue in the CT scan with the module 'segment editor'. The tumour segmentation is also converted to a binary image where tumour is 1 and the other parts are 0. Both segmentations are exported as DICOM file and the orientation and size of the both DICOM files are equal to that of the CT scan.

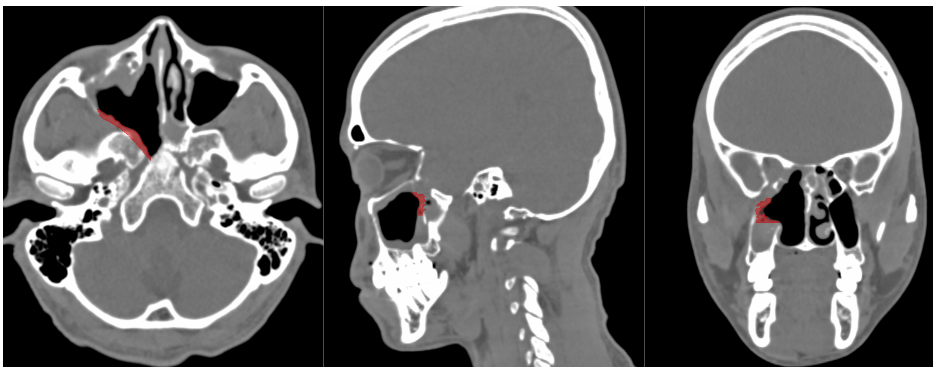

Figure 4.2: Delineation of the tumour/target tissue (red) in 3D slicer.

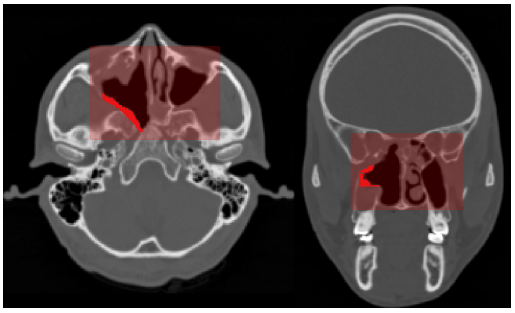

Figure 4.3: Cropping of the CT image, the red box shows ROI.

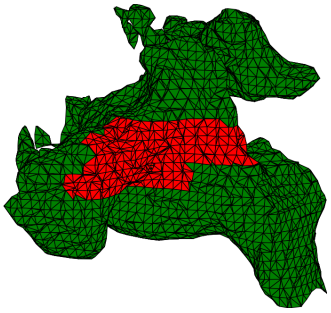

Figure 4.4: Triangular mesh of a sino-nasal cavity with in red the tumour and in green healthy tissue.

4.2.2.2 | Triangular mesh

The sino-nasal cavity of the patient needs to be subtracted from the CT scan. First, the CT scan, segmented tumour and segmented tissue are loaded into Python and the pixels are resized to create isotropic pixels of 1x1x1 mm. All zeros of the segmented tumour are replaced by Not a Number (NaN). This way, an overlay of the segmented tumour can be made on the CT scan. Subsequently, the CT image is cropped manually to remove redundant information, see figure 4.3. The ROI that defines the cropping box should contain the whole sino-nasal cavity. The cropped CT scan is min-max normalised so that the pixel values lay between 0 and 1. A 3D representation of the whole cavity is made by creating a triangular mesh of the cavity wall using the marching cubes algorithm. The contour level is set at 0.1, this pixel value represents the transition from air to tissue in the CT scan. The triangular mesh of a cavity is shown in figure 4.4.

4.2.2.3 | Subspace of Possible light source locations

To determine the OSL it is important to know where the light source can be placed during the cPDT procedure. In consultation with the physician it has been decided that the light source cannot be placed closer than five millimetre to the cavity wall. If the light source lays too close to the wall, it will create a burning spot on the tissue, the five millimetre is a safety margin to protect the tissue.

The set of Possible Source Locations (PSL) is calculated using the tissue segmentation out of the CT scan. For each voxel, the shortest euclidean distance ($Eucl$) from air to tissue is calculated. The Euclidean distance is defined as the straight line distance between two points. The Euclidean distances of each voxel to the cavity wall are stored in an array. The Euclidean distance map can now be created, see figure 4.5. The set of PSLs consists of all voxels that have an euclidean distance larger than five millimetre ($PSL = Eucl > 5$).

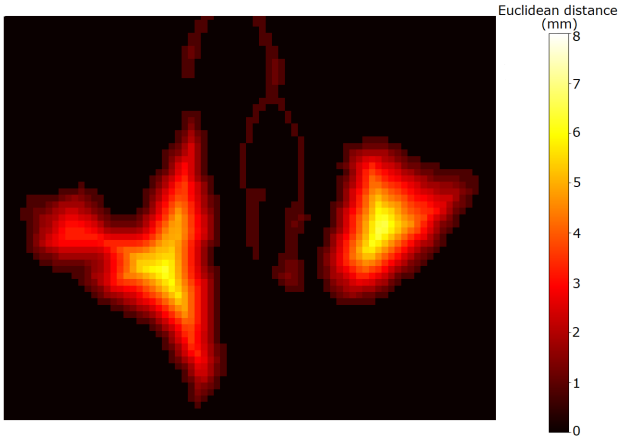

Figure 4.5: An example of the Euclidean distance map with the colour-map on the right. The black background indicates the location of the tissue and the red/yellow pixels indicate the location of the cavity. The Euclidean distance from each pixel to the closest tissue pixel is calculated and is indicated in this Euclidean distance map.

4.2.2.4 | Optimisation

The next step in the planning algorithm is the determination of which location and output power give the best possible results of the PDT treatment. Using mathematical optimisation, the best solution can be found out of a set of feasible solutions. Optimisation methods can solve quantitative problems and is used in a lot of different disciplines, for example in economics, engineering and in medicine (plannings for radiation therapy for example). During an optimisation, a function (the objective function) will be minimised or maximised by adjusting the input values. The values that give the lowest or highest (depending on a minimisation or maximisation) are the result of the optimisation.

Objective function

To be able to give an answer on which location and output power give the best possible results for the patient during cPDT, the problem needs to be converted into a quantitative problem. This is done using an objective function or so called cost function. The criteria that are important to solve the problem are defined in this objective function. The objective function calculates the costs given a source location (SL) and an output power (S). The optimisation will, in this case, minimise the costs.

The goal of the optimisation is to find a combination of an SL and S that illuminates the cavity according to the requirements in section 4.2.1. These requirements are incorporated into the objective function by calculating a cost term for the tumour tissue (Ct) and for the healthy tissue (Ch), see figure 4.6. The costs terms are dependent on the slope of the equation α_h and α_t, the fluence rate on the face (ϕ) and the percentage of

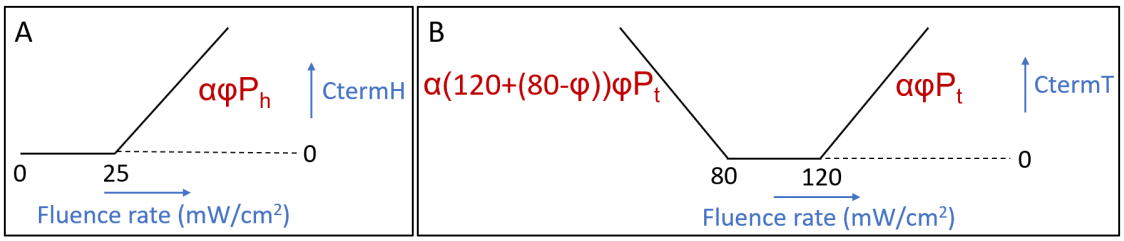

Figure 4.6: Calculation of the 2 cost terms. A: the costs for the healthy tissue and B: the costs for the tumour tissue.

the surface area of the face (P_h and P_t). Furthermore, the objective function consists of a penalty value for the location of the light source. As mentioned in section 4.2.2.3, the light source must be part of the cavity and should not lay too close to the cavity wall. If the SL is part of the PSL, the penalty value (f) will be zero, else the penalty value will be $1e^{15}$. The total costs are calculated by adding the two cost terms, Ch and Ct, and the penalty value f. The weight factors γ_h and γ_t can be used to adjust the cost function. If γ_h is higher than γ_t, the healthy tissue will be more important during the optimisation. If γ_h is lower than γ_t, it is the other way around. The pseudo code of the objective function can be found in algorithm 3.

Optimisation methods

The optimisation problem stated in this research has $4n$ variables, with n the amount of light sources placed during the cPDT procedure. In this research, a maximum of two light sources is used, resulting in a maximum of eight variables. These variables are the x, y and z coordinate of the light source and the output power. Each variable has its own lower and upper boundary. The boundaries for the x, y and z coordinates are defined by the minimum and maximum coordinate of the segmented sino-nasal cavity. The possible variable values are stored in the solution space. The optimisation method should search through the solution space for the solution which gives the lowest costs. There are different methods to search through this solution space. For each optimisation problem a different optimisation method will be the best.

Optimisation algorithms can be classified as deterministic or stochastic algorithms. Deterministic algorithms will give the same output every time when the same initial value is given. A random factor is implemented in stochastic algorithms, so every time the algorithms is run, a different solution can be found. Deterministic algorithms need a good initial estimate and cannot handle multi-objective optimisation problems. Some optimisation methods will easier reach a local minimum and other algorithms intend to reach the global minimum. A lot of algorithms are based on the gradient of the objective function, but sometimes information about this gradient is not available [53–55].

Algorithm 3 Objective function

Require:

$SL1, S1, A_t, A_h, Eucl$ (optional: $SL2, S2$) ▷ with $A_t and A_h$ the area of the tumour and healthy faces

Ensure:

$Costs$

Step 1: Calculate the fluence rate at each face (ϕ) given the location of the light source ($SL1$) and the output power ($S1$) with the empirical light distribution model. The distinction between one and two light sources is made ($SL2$ and $S2$).

if $SL2$ and $S2$ are True **then**
  $\phi \Leftarrow Empirical(SL1, S1) + Empirical(SL2, S2)$
else
  $\phi \Leftarrow Empirical(SL1, S1)$
end if

Step 2: Calculate the cost term for healthy faces. Faces with a fluence rate below 25 mW/cm^2 get an error value of zero. The error value for the other faces depends on the area of the face (A_h) and with how much the threshold of 25 is exceeded.

$A_{h,total} \Leftarrow sum(A_h)$
for each healthy face (i) **do**
  if $\phi[i] > 25$ **then**
    $P_h \Leftarrow \frac{100 A_h[i]}{A_{h,total}}$ ▷ with P_h the percentage of surface area of that face
    $C_h[i] \Leftarrow \alpha_h P_h \phi[i]$ ▷ With C_h the costs of that face
  else
    $C_h[i] \Leftarrow 0$
  end if
end for
$TotalC_h \Leftarrow sum(C_h)$

Step 3: Calculate the cost term for tumour faces. Faces with a fluence rate between 80 and 120 mW/cm^2 get an error value of zero. The error value for the other faces depends on the area of the face (A_t) and with how much the threshold is exceeded.

$A_{t,total} \Leftarrow sum(A_t)$
for each tumour face (j) **do**
  if $\phi[j] < 80$ **then**
    $P_t \Leftarrow \frac{100 A_t[j]}{A_{t,total}}$ ▷ with P_t the percentage of surface area of that face

$C_t[j] \Leftarrow \alpha_t P_t(120 + (80 - \phi[j])$ ▷ With C_t the costs of that face
else if $\phi[j] > 120$ **then**
$P_t \Leftarrow \frac{100 A_t[j]}{A_{t,total}}$
$C_t[j] \Leftarrow \alpha_t P_t \phi[j]$
else
$C_t[j] \Leftarrow 0$
end if
end for
$TotalC_t \Leftarrow sum(C_t)$

Step 4: Calculate error value (f) for SL using the set of possible source locations ($Eucl$).
if $Eucl[SL1] < 5$ **then**
$f \Leftarrow 1e^{15}$
end if
if $SL2$ and $S2$ are True **then**
if $Eucl[SL2] < 5$ **then**
$f \Leftarrow 1e^{15} + f$
end if
end if

Step 5: Calculate the total costs.
$Costs \Leftarrow \gamma_h C_h + \gamma_t C_t + f$

In this research, the performance of two different algorithms is tested, a Grid search and Differential Evolution (DE) method. These methods are chosen after a short evaluation of different optimisation methods. First, a Grid search is used which calculates the cost function of manually chosen solutions and is part of the deterministic optimisation algorithms. This method is really easy to implement and will always find a solution. The main drawback of this optimisation algorithm is the calculation time. If the complexity of the problem increases, the calculation time will also increase excessively.

The Grid search method that is used in this research is based on the creation of multiple 3D grids, see figure 4.7. The first grid consists of 48 points evenly spread over the 3D space in which the triangular mesh is located. The x, y and z coordinate of the grid points are the x, y and z coordinate of the light source. These grid points are used as input for the objective function. The output power is set at a fixed value. The costs at each location are evaluated and the point with the lowest costs is saved. Around this point, a new grid is created that is also used to evaluate the costs at each grid point. This cycle of creating a new grid is performed five times. The grid point with the lowest costs from the last grid (the 5^{th} is the output of the optimisation. This whole procedure

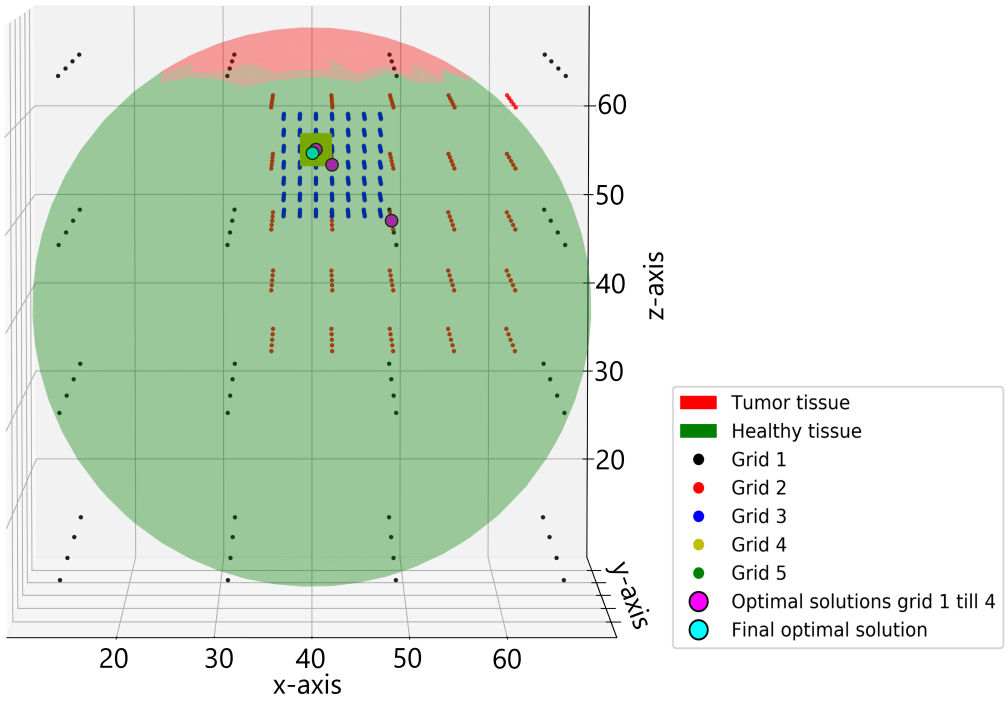

Figure 4.7: Example of the Grid optimisation. Five grids are created (black, red, blue, yellow, green) spread over the 3D space. The optimal solutions per grid is shown. The red part of the circle is defined as tumour tissue and the green part as healthy tissue.

of creating the five grids is performed multiple times for different output powers (from 100 to 1500 with steps of 100).

The second optimisation algorithm that is evaluated in this research is the DE method. This algorithm is an evolutionary algorithm, it uses crossover and mutation to modify a population to eventually reach the global optimum. DE is a meta-heuristic and stochastic algorithm, so no assumptions about the problem are made, the algorithm can search very large solution spaces and a random factor is implemented. This random factor is implemented to avoid to reach a local optimum and speeds up the calculation time [56]. The boundary for the output power of the light source using the DE method is set on 100 to 1500 mW.

DE is an algorithm that tries to find an optimal solution by starting with a group of solutions (population). A schematic representation of the steps taken during DE can be seen in figure 4.8. In this example, the population size is nine and the optimal value of two variables (x1 and x2) will be determined. The population is initialised by choosing nine random points in the search space using Latin hypercube sampling, see figure 4.8 number 1. Latin hypercube sampling generates points while remembering in which row and column the points are placed. This way, the sample points are better distributed

over the search space than generating random points without memory [57]. All points of the population are evaluated using the objective function, so the costs at each point is calculated. The size of the population (P) can be adjusted. It is expected that the higher the population size, the higher the chance of reaching the global optimum [54, 58]. However, the calculation time will also be higher. So, a balance between both should be found [56].

Subsequently, the DE algorithm will generate new points (the second population) based on the information of the first population. A difference vector is created between two random points from the first population (figure 4.8 number 2). This difference vector is used to translate another random point (figure 4.8 number 3). The costs of the new point that arises will be compared to the costs of a point in the initial population, this step is called selection. The point with the lowest costs will be part of the second population (figure 4.8 number 4). The length of the difference vector is controlled by the

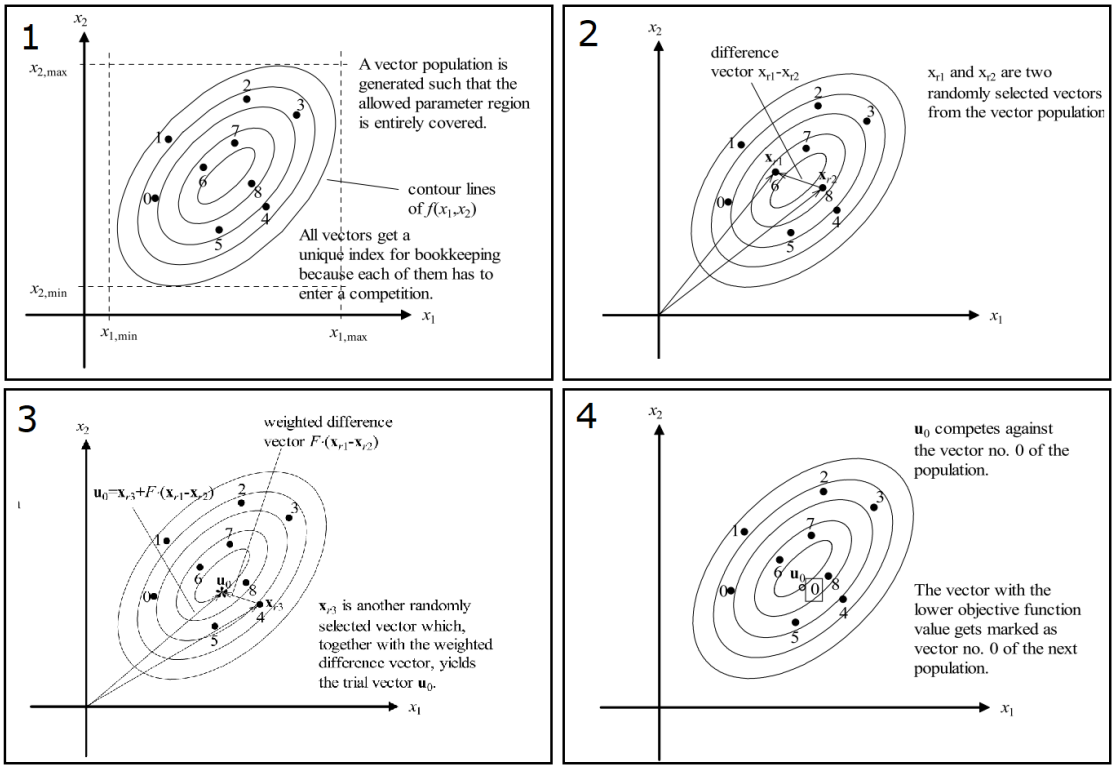

Figure 4.8: Schematic representation of the differential evolution optimisation. 1. Shows the initial population in the solution space of two variables. The contour lines of the objective function are also plotted. 2. Generation of the difference vector. 3. Mutation. 4. Selection [56].

mutation constant (F). This constant consist of a lower and upper value which can be chosen in the range [0,2]. A higher F will lead to a higher chance of reaching the global optimum instead of the local optimum, but will also lead to a higher calculation time. When F is higher, a bigger search field is evaluated during the optimisation.

To decrease the chance to end in a local minimum, the DE algorithm can also perform crossover to create a new population, see figure 4.9. Crossover takes place after the mutation step and before the selection procedure. When a random point is translated to a new point with the difference vector ($\mathbf{v}_{i,g}$), there is a possibility that crossover takes place. This means that a random other point ($\mathbf{x}_{i,g}$) is chosen from the population, the coordinates of the new point ($\mathbf{u}_{i,g}$) are a combination of $\mathbf{v}_{i,g}$ and $\mathbf{x}_{i,g}$. During the selection step, $\mathbf{x}_{i,g}$ will be compared with a point of the initial population. The chance that crossover takes place is dependent on the crossover probability factor Cr which can be chosen in the range [0,1]. Each time, a random value between 0 and 1 is generated. When this random value is less or equal to Cr, then the mutated point is used for the selection. When the random value is higher than Cr, crossover will take place. The higher Cr, the chance that crossover will take place is lower. This means that the chance of reaching a global minimum will be lower and that the calculation time will also be lower. A smaller search field is evaluated using a lower Cr.

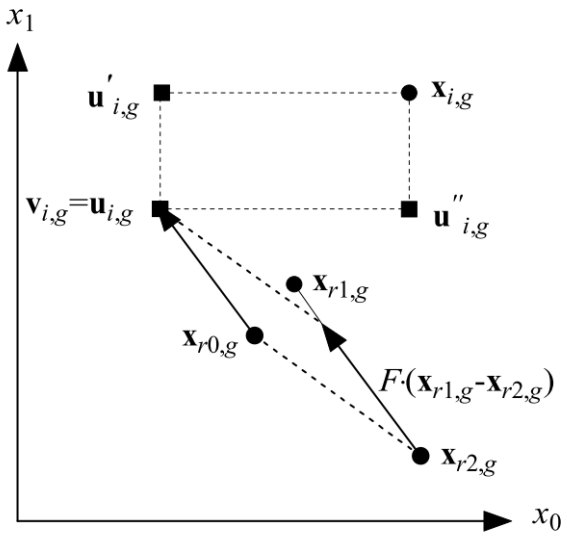

Figure 4.9: Schematic representation of crossover. The mutated point $\mathbf{v}_{i,g}$ will be crossed with a random point of the initial population $\mathbf{x}_{i,g}$ to create a new point $\mathbf{u}'_{i,g}$ or $\mathbf{u}''_{i,g}$ [56].

4.2.3 | Analysis

The Grid optimisation and DE will give the OSL and its output power. The quality of the optimisation depends on various things, such as the objective function and the settings of the optimisation method. For the cPDT planning tool, the settings of the optimisation method that give the best output should be used. First, four parameters of the objective function are adjusted and its best value is chosen. Second, the hyper-parameters of DE, settings that can be adjusted manually, are tested. Third, a comparison between the Grid optimisation method and the DE is performed. CT scans of four patients are used for the analysis of the cPDT planning tool.

The output of the optimisation is assessed on the percentage of surface area of the tumour that has a fluence between the 80 and 120 mW/cm^2 (*Tumour*%), the percentage of healthy tumour that has a fluence below the 25 mW/cm^2 (*Healthy*%) and the calculation time. Ideally, *Tumour*% and *Healthy*% are both 100% and the calculation time should be as low as possible. All optimisations are performed on one computer with Intel core i5-8250 CPU 1.60GHz (4 cores), 8 GB RAM, x64-processor. The optimisation is performed using the empirical light distribution model and a build-up function determined for porcine tissue which is equal to $0.13R_d + 1$.

4.2.3.1 | Optimisation of parameters of the objective function

Four parameters can be adjusted in the objective function which have influence on the result of the optimisation. Suitable values of these parameters must be selected. These four parameters are two weight factors (γ_h and γ_t) and the slope of the two cost terms (α_h and α_t). The values of these parameters which are tested in this research, are defined in table 4.1. The values of each parameter are chosen by trial and error. These 19 different objective functions are tested on CT scans of four patients using DE. The outcome of the optimisation is evaluated by looking at the *Tumour*% and *Healthy*%. The *Tumour*% is the most important factor, it should be as high as possible.

Table 4.1: Settings objective function

#	1	2	3	4	5	6	7	8	9	10	11	12	13	14	15	16	17	18	19
γ_h	1	1,5	2	2,5	3	3,5	4	1	1	1	1	1	1	1	1	1	1	1	1
γ_t	1	1	1	1	1	1	1	1,5	2	2,5	3	3,5	4	1	1	1	1	1	1
α_h	2	2	2	2	2	2	2	2	2	2	2	2	2	4	8	2	2	4	8
α_t	2	2	2	2	2	2	2	2	2	2	2	2	2	2	2	4	8	4	8

4.2.3.2 | Optimisation of hyper-parameters of DE

DE can be performed using different settings for P, F and Cr. The values of these three so-called hyper-parameters are optimised in this research. The settings of all hyper-parameters are defined in table 4.2. The optimal population size is determined first, this population size will be used for the determination of the optimal mutation constant and so on.

The optimisation of the hyper-parameters is performed for only one patient, namely patient 4. The optimisation is performed five times per setting to see if the chance of reaching a local minimum reduces for a certain setting. The outcomes of the optimisations with different settings for DE are tested on the repeatability and the mean computational time. The optimisation should be about the same every time the OSL and its output power are calculated. Furthermore, it is important that the computational time is as low as possible, but still gives the correct results. After the optimisation of the hyper-parameters, the optimisation for DE is performed ten times per CT scan to see how reproducible the method is. The results are evaluated on the costs and the variations of the OSL and its output power.

Table 4.2: Settings hyper-parameters DE

P	5; 15; 25; 50
F	(0.25, 0.5); (0.25, 1); (0.5, 1); (0.75, 1); (1, 1.25); (1, 1.5); (1.5, 1.75)
Cr	0.2; 0.4; 0.6; 0.8

4.2.3.3 | Grid versus DE

The next step in the analysis is to determine which method is best to use for the cPDT planning tool, the grid optimisation or DE optimisation. This analysis is done using a spherical cavity with a diameter of three centimetre and the sino-nasal cavity of patient 4. One part of the cavity is delineated as tumour tissue. The OSL and its output power are determined using both optimisation methods. Thereafter, both methods are used to see if it is possible to find two light source locations and two output power values that give the optimal light distribution. The outcomes of the two optimisation methods are compared by looking at the values for the *Tumour*%, *Healthy*% and the computational time.

4.3 | Results

4.3.1 | Optimisation of parameters of the objective function

The results of the optimisation with DE and the 19 different objective functions are shown in figures 4.10. The results of patient 1 are only shown in this figure, the results for the other patients showed the same trend, these graphs are shown in Appendix A.1. The maximum *Tumour*% is 100% for patient 1 and the maximum *Healthy*% is 86%.

It stands out that a higher γ_h will lead to a higher *Healthy*% and a lower *Tumour*% (see # 2 till 7). When γ_t is higher than γ_h, *Tumour*% is a lot higher than *Healthy*%. With a γ_t higher than 2, the differences between the results are minimal (see # 8 till 13).

By increasing α_h relative to α_t, *Tumour*% will decrease (see # 14 and 15). The other way around, so when α_t increases relative to α_h, *Tumour*% is higher and *Healthy*% is lower (see # 16 and 17). When an α_h and α_t of both four or eight is used (see # 18 and 19), *Tumour*% is a bit lower than its maximum value and *Healthy*% is 2%.

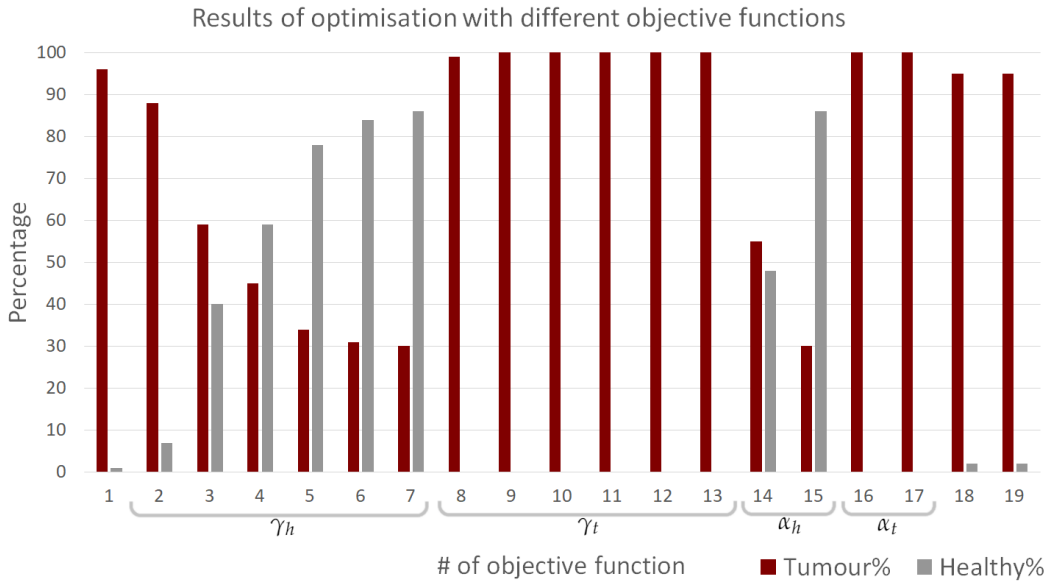

Figure 4.10: Percentage of tumour tissue with a fluence rate between 80 and 120 mW/cm^2 and percentage of healthy tissue with a fluence rate below 25 mW/cm^2 for 19 objective functions for patient 1. The variable that is adjusted in the objective function is indicated below the number of the objective function. If the bar is not visible, the value is equal to zero.

4.3.2 | Optimisation of hyper-parameters of DE

First, the influence of the population size on the results of the optimisation is assessed. These results can be seen in figure 4.11, top left. The costs of the results calculated with a population size of 5 and 15 are very high. The OSL of these optimisations both lay outside the sino-nasal cavity. Using higher population sizes (25 and 50), these high costs did not occur. The mean costs and the standard deviations (SD) using different population sizes are shown in table 4.3. The mean costs and SD are much higher for a population size of 5 and 15 compared to a higher population size. However, when a higher population size is used, the mean computational time increases, see table 4.3.

Second, various mutation constants are used for the DE optimisation, the results are shown in figure 4.11, top right. In this graph and in table 4.3, one can see that the variations between the five measurements decrease using a higher mutation constant. Unfortunately, the computational costs also increase using a higher mutation constant, see table 4.3. The mean computational time is the lowest for a mutation constant of (0.25, 0.5), namely 50 seconds. The mean computational time reaches 655 seconds for a mutation constant of (1.5, 1.75).

Lastly, the crossover probability factor is adjusted and its impact on the optimisation is evaluated, see figure 4.11, bottom left. The higher Cr, the more variations are present in the optimisation and the lower the computational time, see table 4.3.

Table 4.3: Mean costs, standard deviation and computational time per setting of the three hyper-parameters.

Variable	Setting	Mean costs	$\pm$ SD	Time (s)
P	5	4.10^{13}	5.10^{13}	31
	15	4.10^{13}	5.10^{13}	89
	25	38650	35	220
	50	38602	53	478
F	(0.25, 0.5)	37584	4368	50
	(0.25, 1)	34821	215	66
	(0.5, 1)	34887	188	112
	(0.75, 1)	34907	133	162
	(1, 1.25)	35019	146	272
	(1, 1.5)	34913	121	330
	(1.5, 1.75)	35057	110	655
Cr	0.2	34635	2	1700
	0.4	34701	30	311
	0.6	34905	116	155
	0.8	35665	1368	100

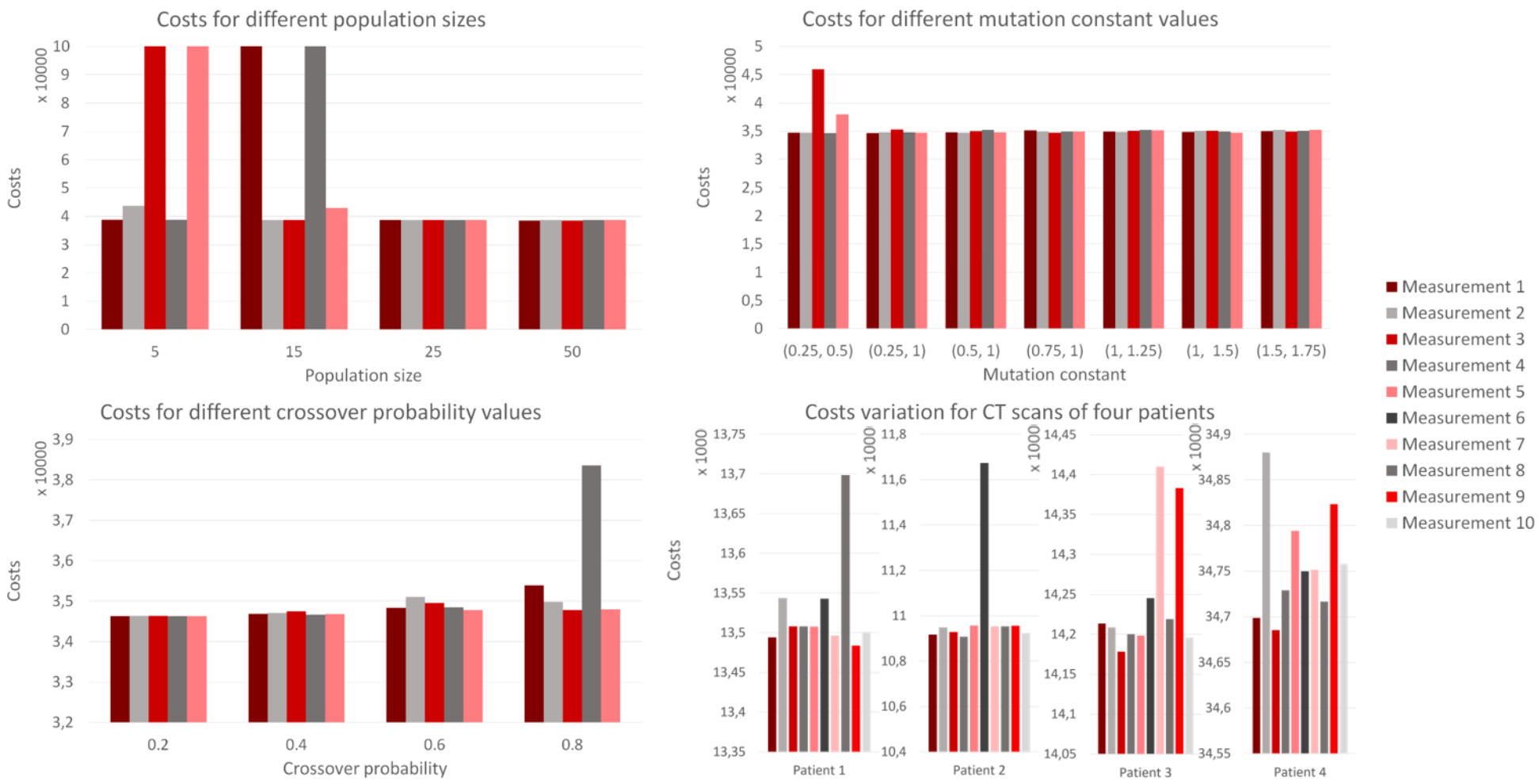

Figure 4.11: Results of the optimisation of the hyper-parameters of DE and the repeatability test. Top left: Results of different population sizes. Top right: Results of different mutation constant values. Bottom left: Results of different crossover probability values. In these three graphs, the costs of the outcome of the optimisation is given on the left y axis and the mean computational time is given on the right y axis. Bottom right: Results of the repeatability test, the optimisation is performed ten times for all four patients, the y-axis is adjusted for each patient.

By evaluating the three settings of DE optimisation, the best settings are chosen by finding a balance between the repeatability and computational time of the optimisation. For the repeatability test, P is set at 15, F at (0.5, 1) and Cr at 0.6, seethe discussion for detailed explanation for these choices. After finding the best settings of DE, the optimisation is performed ten times on CT scans of four patients, see figure 4.11, bottom right. This graph shows that the DE optimisation method with the current settings gives about the same results when it is run for ten times. The costs do not differ a lot between multiple optimisations. The sixth calculation for patient 2 stands out, the costs are a lot higher than that of the other nine calculations for patient 2. The mean costs per patient with its standard deviation and the biggest difference between the ten optimisations in distance from the OSLs and its output power are shown in table 4.4. The big difference of 4.34 mm between the OSLs for patient 2 is a result of the sixth optimisation. When this sixth calculation is not taken into account, the biggest distance between the OSLs for patient 2 would be 0.88 mm. This difference is also noticeable in the tumour coverage. The sixth optimisation for patient 2 resulted in a *Tumour*% of 91% and a *Healthy*% of 25%. All other optimisation for patient 2 resulted in a *Tumour*% of 99 or 100% and a *Healthy*% of 2 or 3%.

Table 4.4: Repeatability test results: optimisation is performed ten times for four patients. The mean costs with its standard deviation (SD), the biggest difference between the ten OSLs per patient and the biggest difference in output power per patient are given.

Patient	Mean costs (SD)	Δ Distance (mm)	ΔS (mW)
1	13528 (60)	0.82	49
2	11012 (221)	4.34	280
3	14245 (78)	1.89	100
4	34759 (57)	0.37	19

4.3.3 | Grid versus DE

The results of these optimisations can be seen in table 4.5. The main difference between both methods is the computational time. The Grid method was able to calculate the OSL and its output power for one source location, however the computational load was too high for two source locations. The optimisation with two light sources was executed for only two different output powers to test the computational time, this took over nine hours. The OSL differs approximately one millimetre between the grid and DE method and the output power differs 85 mW for the spherical cavity.

Table 4.5: Results Grid versus DE optimisation on a sphere with radius of 3 cm and on the sino-nasal cavity of patient 4.

Shape	**Method**	**# locations**	**Costs**	*Healthy%*	*Tumour%*	**Time (s)**
Sphere	*Grid*	1	8856	0	100	199
		2	-	-	-	>32.400
	DE	1	8132	0	100	52
		2	8134	0	100	730
Sino-nasal cavity	*Grid*	1	39129	5	49	525
		2	-	-	-	-
	DE	1	35000	0	70	361
		2	14937	1	93	4058

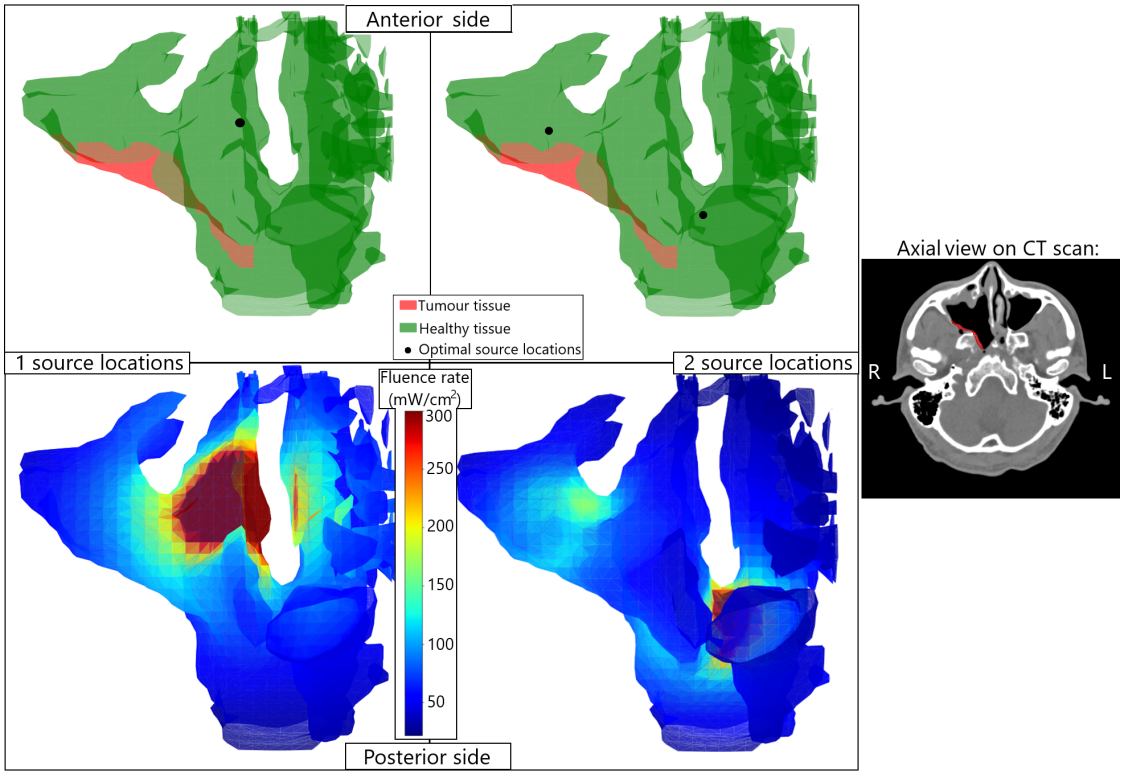

Figure 4.12: OSLs determined with DE optimisation for patient 4. Green part of the mesh are the healthy faces and red the tumour faces. Left: the optimisation with one spherical bulb diffuser. Middle: the optimisation with two spherical bulb diffusers. Right: the CT scan with delineation of the tumour in axial view, the same view as the meshes of the cavity.

The DE optimisation with two light sources did not improve the outcome for the cavity in the shape of a sphere. The costs are about the same for two light source locations compared with one light source location for the DE optimisation method. The Grid method showed higher costs. However, the use of two light sources for the sino-nasal cavity of patient 4 shows great improvement compared to the use of one light source. The results of the optimisation with one and two light sources in the sino-nasal cavity of patient 4 performed with DE optimisation are shown in figure 4.12.

4.4 | Discussion

The aim of this research was to develop a cPDT planning tool that is able to calculate the OSL and its output power ensuring the best possible outcomes of cPDT. The cPDT planning tool that is developed is based on the empirical light distribution model, a CT scan of the patient and the use of a spherical bulb diffuser. In this section, the results are discussed first. After that, the requirements, that are composed in the method of this research, will be assessed. By determining to what extent the cPDT planning tool meets the requirements. Finally, the limitations of this research and recommendations for further research will be given.

4.4.1 | Optimisation of parameters of the objective function

The first sub-goal was to determine which settings of the objective function result in the best outcomes. This was analysed by looking at *Tumour*% and *Healthy*% for the 19 different objective functions. It would be optimal if *Tumour*% and *Healthy*% are both 100%, meaning that all tumour tissue receives a fluence rate between 80 and 120 mW/cm^2 and all healthy tissue receives a fluence rate below 25 mW/cm^2. By looking at the results, none of the objective functions will lead to an optimal *Tumour*% and *Healthy*% during the optimisation. This can be explained by the type of light source that is used. The spherical bulb diffuser emits light isotropic in all spherical directions and is not solely directed to the tumour. Furthermore, *Tumour*% for patient 4 never reaches the 100% contrary to *Tumour*% for the other three patients. This difference can be explained by the delineation of the tumour for the four patients. In Appendix A.2, the delineation of the tumours for all patients is shown. The tumour for patient 4 is much bigger than that of the other patients, resulting in the inability to illuminate the tumour tissue 100% with one spherical bulb diffuser.

Figure 4.10 shows that objective functions # 9 to 13, 16 and 17 give the highest *Tumour*% (100%). However, *Healthy*% is in all these cases equal to zero. During the treatment it is most important to illuminate the whole tumour with a sufficient fluence, the dosis on the healthy tumour is of second interest. Out of these 19 objective functions,

the 9th is chosen to use for the optimisation from this point forward. This 9th objective function has a γ_h of 1 and a γ_t, α_h and α_h of 2.

4.4.2 | Optimisation of hyper-parameters of DE

Using the 9th objective function, an analysis is performed with varying hyper-parameter values of DE. The results of the population size are assessed first. As expected, the computational time increases with a higher population size. The lower the population size, the more variations in the results occur. Two out of five times of the optimisation with a P of 5 and 15, the OSL was outside the cavity. A population size should be chosen resulting in a reasonable computational time and not too much variations between multiple optimisations. Therefore, a population size of 25 is chosen.

By adjusting F, it stands out that less variations can be seen between the optimisations using a higher F. When F is low, a small area of the search field is analysed during the optimisation. The chance is higher that the optimisation ends in a local minimum than when a higher F is used. This will lead to higher variations between the optimisations. The computational time reduces with a lower F. The F of (0.5, 1) is selected as the best balance between the computational time and the variations of the optimisation.

The quality of DE is also assessed with different crossover probability factors. The results are conform the theory behind Cr. The higher Cr, the lower the chance that crossover takes place, resulting in a higher chance of ending in a local minimum. The results show that a higher Cr gives more variations in the optimisation. Again, the computational time varies when a different Cr value is chosen. The higher the chance of reaching a global minimum, the higher the computational time. A bigger search field has to be evaluated to reduce the chance of reaching a local minimum, resulting in a longer computational time. The Cr is set at 0.6, because the variations between five optimisations is minimal and the computational time is still acceptable.

Lastly, the optimisation is performed 10 times per patient using the hyper-parameter values chosen in this research. The variation between ten measurements for four patient are minimal. The optimisation did not result in an OSL outside the cavity what did occur with some settings of the hyper-parameters. Most of the DE optimisations resulted in exactly the same OSL and an output power with a few milliwatts difference. The biggest difference in location of the OSL is in patient 2. The quality of the sixth calculation for patient 2 was lower than the others. The variation due to the sixth calculation is equal to an OSL Euclidean distance difference of 4.5 mm and an output power difference of 300 mW. This outlier can be explained by the random factor that is present in the DE optimisation algorithm and will always be present in the algorithm. There will always be a chance that the optimisation will be stuck in a local minimum. However, this chance can be reduced by adjusting the hyper-parameters, for example by up-scaling

the population size. This will reduce the chance of reaching a local minimum, but also will increase the computational time.

The optimisation for the other patients show less variations, with a maximum distance variation of 1.89 mm and output power variation of 100 mW. This observed variation is acceptable, because the navigation system that will be used to place the light source at the planned location during surgery has an accuracy of about 1.5 mm. Therefore, it can be concluded that this optimisation method gives results that are reproducible and can be used for the cPDT planning tool.

4.4.3 | Grid versus DE

The DE optimisation method is compared to the Grid optimisation method to determine which method is the most efficient in the calculation of the OSL and its output power. These optimisations are performed on a sphere with a diameter of three centimetre and the sino-nasal cavity of patient 4. When the optimisation is performed with both methods for one light source, it is immediately clear that the Grid method is less efficient in terms of the computational time. The computational time for the Grid method was about four times the computational time needed for DE using the sphere and 1.5 times using the sino-nasal cavity. The Grid method needs to calculate the costs at a standard number of locations in the search field. The DE algorithm takes into account which position in the search field resulted in the lowest costs at that moment and adjusts its next position keeping the best location in mind. This search method is more efficient than the Grid method. Furthermore, the costs of the OSL and its output power calculated with the Grid method is higher than that calculated with DE using both cavities.

The results of the optimisation with two source locations are conform the results of the optimisation with one source location. It took too long to calculate the optimisation with the Grid method. The amount of variables increases from four to eight when using two light sources instead of one light source. The computational time does increase so much that it is not usable in a clinical setting. The results of using two light sources for a spherical cavity did not show improvement compared to one light source. For the sino-nasal cavity of patient 4, the use op two light sources really did improve the results. The *Tumour*% did increase from 70% to 93%.

Concluding, the DE method gives a lower costs after the optimisation than the Grid method. Furthermore, the computational time is a lot lower and it is possible to calculate the OSL and output power for two light sources within a reasonable time frame. Therefore, the DE optimisation method is chosen to be the best method from these two to solve this optimisation problem.

4.4.4 | Requirements

Considering a planning tool for cPDT based on DE optimisation, the requirements described in section 4.2.1 are evaluated in this section:

1. Determine OSL and its optimal output power:
   The main goal of the planning tool, the determination of the OSL and its output power, is reached. Most of the times it is not possible to achieve the requirements for the illumination of both the tumour and healthy tissue in case of the use of a spherical bulb diffuser. However, the reason for this is often due to limitations of the cPDT equipment such as the light source and not due to the optimisation method.

2. Multiple light sources:
   This cPDT planning algorithm is able to simultaneously calculate the optimal position of two light sources. It is also possible to implement the same procedure for more than two light sources. However, it is not feasible to position a lot of light sources during the treatment. Therefore, the maximum number of light sources is set at two.

3. Reproducible:
   In this study, the repeatability of the optimisation algorithm is tested. In the results, one can see that the performance of the algorithm does not vary very much within ten repetitions. There will always be a random factor present in the planning tool, therefore variations will always be present.

4. User friendly interface:
   The cPDT planning tool does not yet have a user friendly interface. This is needed to be used in a clinical setting and will be the priority if the cPDT planning tool is completed.

5. Implementation in the operation room:
   The cPDT planning tool is not yet implemented in the clinical workflow. For more information about the clinical implementation and challenges that arise with this implementation see chapter 6.

6. Computational time:
   The time to calculate the OSL and its output power depends on the number of source locations that are used. The optimisation with two light sources does generally not take longer than 15 minutes. This is computational time is reasonable, especially considering the use of a laptop in this research which can be replaced with a more advanced computer.

4.4.5 | Limitations and recommendations

There are some limitations of this research that influence the results and which can be improved in further research. First, the limitations of this research that are based on the optimisation will be discussed. Subsequently, more general limitations that are focused on the empirical light distribution model will be appointed.

The optimisation method that seemed most suitable in this research, differential evolution, is efficient in solving the optimisation problem. DE optimisation gives good results within a reasonable time range and the results are reproducible. However, there are multiple other optimisation methods available which could be more efficient than DE. During this research, other possible optimisation methods are shortly tested and evaluated before the DE algorithm was selected. Among these optimisation methods were dual annealing (DA) and Simplicial Homology Global Optimisation (SHGO) [59]. After a short assessment, the results of DE appeared superior to the other optimisation methods. More research could be done to find other optimisation methods that are more efficient than DE.

Furthermore, the optimisation of hyper-parameters of DE are assessed using a CT scan of one patient. It is possible that the hyper-parameters selected in this study can only be applied on this patient and that they are not general for all patients. For example, in case of the population size, it is possible that the optimal population size depends on the size of the cavity. The bigger the cavity, the higher the population size should be. However, the repeatability test is performed on four patients and showed little variations between multiple calculations.

In this research, three hyper-parameters are optimised empirically. However, there are more adjustments that can be made to improve the performance of the differential evolution optimisation. A lot of modified DE algorithms are developed and the performance is tested [60–62]. The basic optimisation method that is described in this research shows promising results. It is possible that one of the modified DE algorithms that are already developed will improve the optimisation of the cPDT planning.

Another limitation is the analysis method of the different objective functions. This analysis is based on *Tumour*% and *Healthy*%. Nonetheless, these parameters only indicate if the hard limit of 25 mW/cm^2 is exceeded in case of *Healthy*% and do not give a value on how much this limit is exceeded. This really is of great importance in the analysis of the optimisation. The OSL that is calculated with the optimisation should be assessed on *Tumour*% and *Healthy*%, but how much the limit is exceeded should also be part of the evaluation in further research.

The set of PSLs is determined by defining the area in which the Euclidean distance from the cavity to the wall of the cavity is bigger than five millimetres. The light source can not be located outside this area. This is taken into account in the objective function, an error value will be given to locations that lay outside this area. This is, however, not

an efficient way of performing the optimisation. The bounds of the x, y and z coordinate of the source location are the minimum and maximum coordinate of the segmented cavity. It would be better if the bounds of the source location are based on the set of PSLs and not only on the size of the segmented cavity. This way, the optimisation will not spend time on calculating the costs of a source location that is located outside the cavity and this will lower the computation time.

The OSL that is calculated with the optimisation is part of the PSL. However, some locations in the cavity cannot be reached during surgery because there is no clear way to navigate the light source to this location. It is recommended that the physician can indicate which locations in the cavity are reachable with the light source during cPDT. Only these locations should be the input of the PSL.

The other limitations of the cPDT planning tool are mainly based on the light distribution model that is used. This cPDT planning tool is based on the empirical light distribution model. This model can calculate the light distribution in the cavity very fast, but is not able to determine if some parts of the cavity lay in a shaded area. The illumination is only based on the distance between the light source and the face. The fluence rate is the same for faces located in shaded areas and for faces that receive direct illumination. This might introduce a larger error in the determination of the optimal light source location and its output power. The analytical model is able to determine the location of shaded areas and this script can also be used in the empirical model. However, this calculation is based on ray-tracing and is not efficient. Implementing the ray-tracing algorithm will lead to a tremendous increase in computational time of the optimisation. Future research should focus on the creation of a more efficient script for the determination of shaded areas. Also, the possibility of implementing the analytical light distribution model in the cPDT planning tool should be determined.

The inability to calculate shaded areas with the current version of the empirical model gives misleading results of the optimisation. The OSL and its output power are calculated without taking the shaded areas into account. The *Tumour*% and *Healthy*% that is calculated and shown in the results of this research do not represent reality. In fact, *Tumour*% will be lower and *Healthy*% will be higher than calculated due to the shaded areas. The OSL and its output power should be used to calculate the light distribution with the analytical model which gives a better representation of the reality.

Moreover, the empirical model that is used for the cPDT planning tool is still based on a linear build-up function. In chapter 3, it is concluded that it is better to describe the β factor with a quadratic function instead of a linear function. This quadratic function is not yet implemented into the cPDT planning tool. More research should be done to validate this quadratic function before it can be used in the cPDT planning. Using the quadratic build-up function will result in a different light distribution in the cavity. However, it is not expected that another build-up function will lead to a difference in

the performance of the cPDT planning tool.

Lastly, this cPDT planning tool is able to calculate the OSL and its output power for a spherical bulb diffuser. Though, there are multiple types of light sources available during cPDT, such as the microlens. A microlens can focus the light on a specific area of the tissue and ensure a lower fluence on surrounding tissues. However, the light distribution models are only validated for a spherical bulb diffuser. Therefore it is up till now not possible to determine the OSL and its output power using different types of light sources. A first step in the implementation of a microlens in the light distribution models is made in chapter 5. After validation of this light distribution model, it can easily be implemented into the cPDT planning tool. Eventually, the cPDT planning tool should be able to indicate which type of light source will ensure the best illumination of the tumour.

4.5 | Conclusion

The main goal of the current study was to develop a planning tool for the treatment of superficial sino-nasal carcinomas with cPDT to ensure a good response of the tumour and reduce the side effects. The cPDT planning tool that is developed, shows promising results. The differential evolution algorithm is superior to the Grid search optimisation method based on the computational time. The DE algorithm, introduced in this study, is able to determine the best location of maximal two light sources and its corresponding output power. The main limitations of this study are based on the light distribution model that is used for the planning tool. Further research is required to develop a fast light distribution model that is able to calculate shaded areas and in which multiple types of light sources can be implemented.

5 Microlens

5.1 | Introduction

The empirical and analytical light distribution models that are developed in earlier research, are able to calculate the light distribution in a sino-nasal cavity using a spherical bulb diffuser. However, the spherical bulb diffuser sometimes does not give the desired light distribution due to the isotropic emitted light around the bulb. The light source cannot emit its light directly and targeted at the tumour tissue. Therefore, multiple other light sources are available for the treatment of superficial tumours with cPDT. One of these is the microlens, which is a frontal light distributor, see figure 5.1. This type of light source is able to illuminate a part of the tissue more specifically. This will lead to less damage to the surrounding healthy tissue and thus reduces the side effects that occur due to PDT [33, 63].

In this chapter, the first steps towards the implementation of the microlens into the empirical light distribution model is made. First, the specifications of the microlens are elaborated, second the algorithm that is created to simulate the light distribution is described and third recommendations for further research are given.

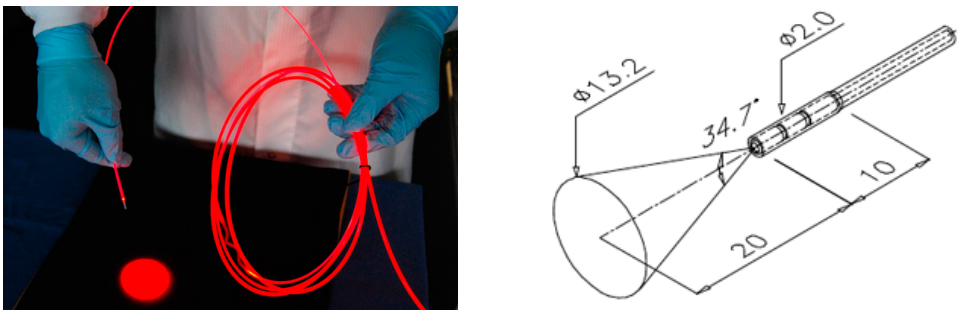

Figure 5.1: Left: The microlens light source illuminates a surface with a circular spot [64], Right: Schematic representation of the microlens [63].

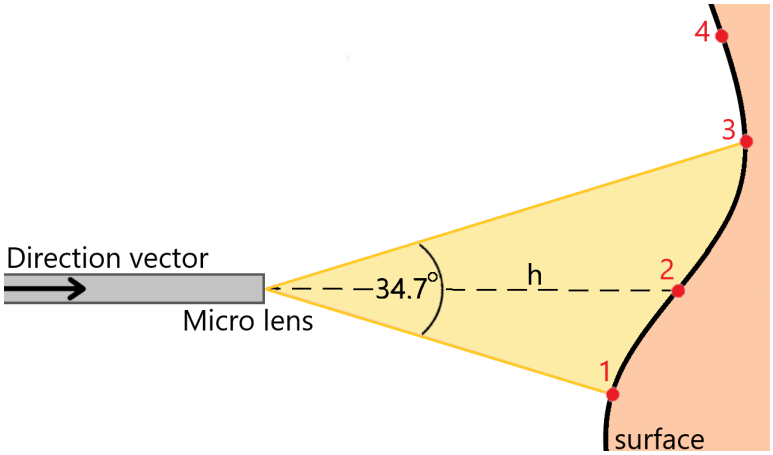

Figure 5.2: Schematic representation of the illumination of a surface with a microlens. The microlens has a outgoing light beam with angle δ of 34.7° and a direction vector indicating the orientation of the microlens. The distance from the microlens to the surface (h) determines the fluence rate at each location (1, 2, 3 and 4).

5.2 | Microlens specifications

The microlens is also called a frontal light distributor. The diameter of the fiber is two millimetre and can therefore also be used through the working channel of an endoscope, see figure 5.1, the right image. The microlens creates a uniform circular spot of light. The diameter of this spot depends on the angle of the outgoing light beam (δ) which is in this case 34.7° and the length of center line of the light beam (h), see figure 5.2. The light beam radius at different lengths h can be calculated using equation 5.1.

$$R = htan(\frac{\delta}{2}) \tag{5.1}$$

Where R is the radius of the spot, h the length of the centre line of the light beam and δ the angle of the outgoing light beam which is in case of the medlight microlens 34.7°.

The fluence rate is similar at each location in the spot with the same h. A smaller R will lead to a higher fluence rate inside the spot, see equation 5.2.

$$\phi_{inc,lens} = \frac{S(Ah+1)}{\pi R^2} \tag{5.2}$$

Where $\phi_{inc,lens}$ is the fluence rate inside the circular spot, S is the output power of the light source, A is the slope of the build-up function.

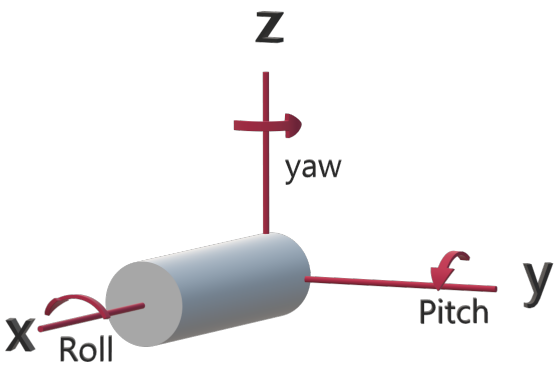

Figure 5.3: The orientation of the microlens (grey cilinder) in a 3D coordinate system. The pitch and yaw describe the location of the illuminations spot. The roll is not of importance.

Figure 5.2 gives a schematic representation of the illumination of a surface with the microlens. The fluence rate at position 1 is higher than that at position 2 and 3 due to the spread of the same energy on a larger spot (h is larger at position 2 and 3 than at position 1).

Another important thing to take into account with the implementation of the microlens in the empirical model is the direction of the microlens. The direction of the spherical bulb diffuser is not of importance due to the isotropic distribution of the light. However, the microlens directs its light beam in a certain direction. A direction in a three dimensional space can be described with a normalised direction vector which has two degrees of freedom, see figure 5.3. For the location of the spot, the yaw and pitch are important and both can take values from 0 to 360°.

5.3 | Algorithm

The light distribution in the sino-nasal cavity using a microlens can be determined in a few steps. First, it is important to know which faces are laying inside the spot and which lay outside the illumination spot. The faces can be divided into two groups based on if they receive incident light or not. Second, the fluence received by these faces can be calculated.

5.3.1 | Inside beam or not?

To determine if a face lays inside or outside the light beam, the direction of the microlens and the length of the centre line of the beam (h) should be known. The direction of the microlens can be indicated using the degrees of the yaw and pitch. The angles of the yaw and pitch are converted to a normalised directional vector ($\vec{dir}$), see equation 5.3.

$$\vec{dir} = [cos(yaw)sin(pitch), sin(yaw)sin(pitch), cos(pitch)] \tag{5.3}$$

Where $\vec{dir}$ is the normalised directional vector in the form [x, y, z], yaw the angle of the yaw movement, pitch the angle of the pitch movement.

The next step is to determine if the face lays inside the beam or not. This can be determined using the length of the centre line of the beam (h) and the radius of the spot at that location, see figure 5.4. The location of the centre of each face can be described with a vector ($\vec{p}$). The length of the projection of $\vec{p}$ on $\vec{dir}$ is equal to h. The projection can be calculated with the dot product. The radius (R) of the spot at h can be calculated using equation 5.1. If the orthogonal distance from the centre line of the light beam to the centre of the face is smaller than the radius of the light beam at that location, the face will lay inside the light beam. Otherwise, the face lays outside the beam and does not receive initial light from the microlens. The orthogonal distance can be calculated using the angle δ and the distance D between microlens and the centre of the face, see figure 5.4.

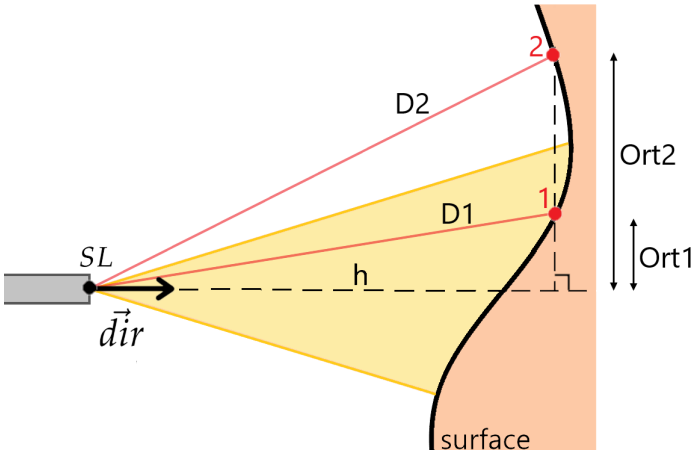

Figure 5.4: The centre points of two faces (1 and 2) and the distances that are needed to determine if the faces lay inside or outside the light beam. SL = location microlens, $\vec{dir}$ = directional vector, h = length of centre line of the light beam, D1 and D2 = distance between SL and point 1 and 2 respectively, Ort1 and Ort2 = orthogonal distance.

5.3.2 | Fluence rate calculation

The faces inside the light beam receive initial light from the microlens. The fluence rate on the faces inside the spot receive a fluence rate as calculated with equation 5.2. The slope of the build-up function for faces inside the spot is described with A_i.

The calculation of the fluence rate that is received by the faces that lay outside the light beam is more difficult. Tan et al. showed that scattering leads to a high build-up of fluence on parts of the tissue that lay outside the light beam [65]. Therefore, the fluence rate at faces outside the light beam should also be determined.

The initial light that reaches the faces inside the light beam will be scattered back into the cavity. In this first set up, it is assumed that the cavity is illuminated following the principles of a spherical bulb diffuser with the output power equal to the total backscattered light, see figure 5.5. First, the mean location of all faces that receive initial light is calculated (the center of the spot). Second, the output power of the microlens is multiplied with the reflection coefficient (Rd) to determine the amount of light scattered back into the cavity ($S_{scatter}$). The fluence rate at the faces outside the light beam is calculated using equation 5.4.

$$\phi_{outside} = \frac{RdS(A_o r + 1)}{2\pi r^2} \tag{5.4}$$

Where $\phi_{outside}$ is the fluence rate at the faces outside the light beam, RdS is the total scattered light by the faces inside the light beam, A_o is the slope of the build-up function for faces outside the spot and r is the distance from the center of the spot from where the scattered light is sent back into the cavity to the centre of the face.

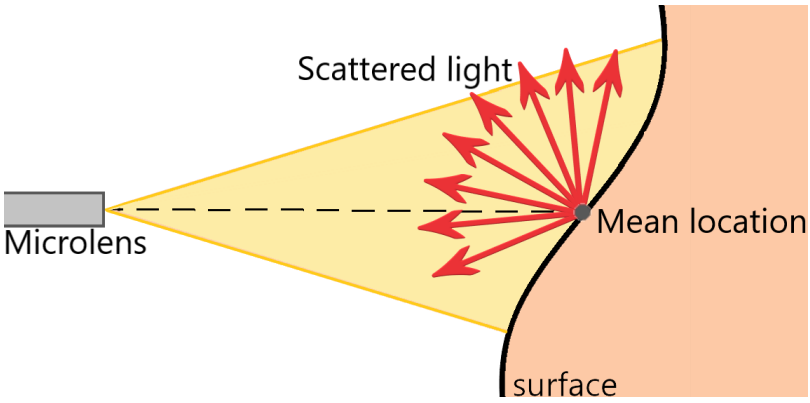

Figure 5.5: The incident light is scattered back into the cavity from the mean location of all faces receiving incident light. The light distribution is assumed to follow the principles of a spherical bulb diffuser.

The build-up function has be determined for the use of a spherical bulb diffuser and not yet for the microlens. Some measurements that are performed earlier on a 3D printed phantom of a sinonasal cavity are used to estimate a linear build-up function using a microlens. The estimation for A_i is 0.05 and of A_o 0.4 using the sinonasal cavity of one patient.

The light distribution in a sphere is calculated with the algorithm that is developed. The difference between the faces inside and outside the spot are clearly visible, see figure 5.6. Furtheremore, the fluence rate differences inside the spot are visible. For the calculation of this light distribution, an output power of 100 mW is used with the estimation of A_i and A_o of respectively 0.05 and 0.4.

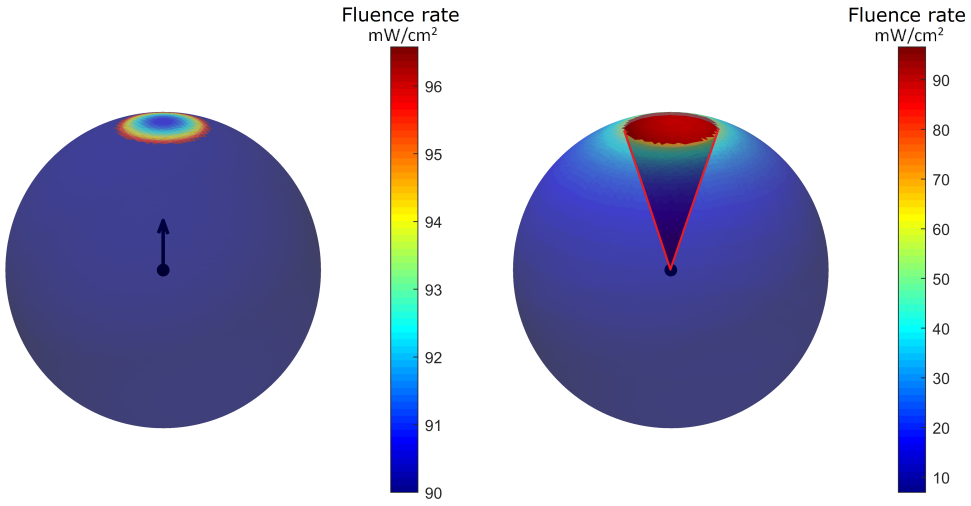

Figure 5.6: Light distribution in a cavity using a microlens. The left image shows the light distribution inside the spot. The black dot and arrow indicate the location of the microlens and its directions. The right image indicates the light distribution in the whole cavity where the black dot indicates the location of the microlens and the contour of the light beam is indicated with red lines. Both images have its own colour bar on the right of the light distribution. The black dot in the middle of the sphere is the location of the microlens and the red cone simulates the light beam.

5.4 | Recommendations for further research

In this chapter, the first steps towards the implementation of a microlens into the light distribution models is made. The algorithm that is created up till now is elaborated and the light distribution in a sphere is shown. The developed model has some limitations which should be improved in further research.

The created algorithm is based on the theories that are currently known about the light distribution in a cavity. The light distribution model for the microlens is not yet verified. In further research, measurements should be performed to test if the algorithm is able to predict the light distribution in the cavity sufficient. These measurements have to be performed in a sino-nasal phantom model using a microlens. The microlens and measurement probes should be positioned at a known location. This way, the measurements can be compared with the results of the light distribution model. Some measurement probes have to be located inside the spot and some outside. These measurements should be used to determine what the build-up function looks like for faces inside and outside the spot. The build-up function is now estimated using a few measurements, but more measurements are needed to determine the exact build-up function. Also, it is not known if the build-up function can be described with a linear equation as it is done currently.

In this light distribution model, it is assumed that the faces that do not receive initial light do receive scattered light from the faces inside the light beam. This theory is implemented in the model by combining the total initial light dose. This total light dose is set as the output power of a 'new' virtual light source that is located at the mean location of all faces inside the light beam. This virtual light source simulates an isotropic distribution of the scattered light through the cavity. This way of implementing the scattered light is a simplification of the truth. An improvement of this implementation could be to simulate the distribution of the scattered light using a surface fluence rate model instead of an isotropic distribution. Using a surface fluence rate model implies that the surface of the cavity can be described as a Lambertian surface. The scattered light will not be distributed isotropically, but following the Lamberts cosine law, see the explanation in section 2.2.

Eventually, when the light distribution model for the microlens is verified, it should be implemented into the optimisation algorithm. The outcomes of the optimisation between the spherical bulb diffuser and the microlens have to be compared. Ideally, the cPDT planning algorithm gives which light source ensures the best light distribution on the tumour tissue. This implementation of the microlens into the cPDT planning algorithm causes however other possible issues. The cPDT planning algorithm will give the optimal location of the microlens, but also the direction that the micro lens should have to illuminate the tumour. This position and direction should be reached during the cPDT procedure with the navigation system. However, it is difficult to indicate what the direction of the microlens should be with the navigation system. The navigation system that is currently used can only show predefined dots in the CT scan, a direction cannot be indicated. More research should be done to find a way to position the microlens adequate during cPDT.

6 Clinical Implementation

In this thesis, a cPDT planning tool is developed that is able to determine the optimal light source location and its output power ensuring the best possible results of cPDT. This planning tool determines the location of the light source using a CT scan of the patient, an air versus tissue segmentation and a delineation of the tumour. The question that arises next is, how can this location be reached during surgery and what is needed to eventually be able to use this cPDT planning tool. This chapter focuses on the whole clinical workflow that is needed to implement the cPDT planning tool and the challenges that arise will be addressed.

First, the patient selection will take place, this will be exactly the same as it is performed currently, see section 1.3.6. It is important that a CT scan of the head and neck area is available of each patient. Second, the physician has to delineate the location of the tumour on the CT scan and an air-tissue segmentation needs to be created. The delineation of the tumour by the physician is now done using the CT scan and 3D Slicer 4.10.1. However, this is not the most optimal method to delineate the tumour. Often, the tumour is too small to be noticeable on the CT scan. It would be better if the tumour could be delineated using an endoscopic view. Weersink et al. demonstrated a method to improve superficial target delineation by tracking an endoscope and registration with the CT scan [66]. With an endoscope, the small superficial tumour is easier to distinguish from healthy tissue. This method can maybe be used in the future to delineate the tumour more easily.

Subsequently, the CT scan, delineation of the tumour and the air-tissue segmentation are used to make the patient specific cPDT planning. Prior to the planning that will be performed, the values of some patient specific variables need to be determined. The empirical light distribution model can calculate the light distribution based on the distance from the light source to the surface and the build-up function. After some more research, the build-up function can hopefully be determined using the dimensions of the sino-nasal cavity and Rd, see chapter 3. The dimensions of the sino-nasal cavity can be calculated using the air-tissue segmentation of the CT scan. The volume and/or surface area can easily be calculated. The determination of the patient specific Rd value is

more challenging. This should be done by performing measurements in the sino-nasal cavity. Therefore, it is easier to determine a mean *Rd* value for all patients. Research is currently performed to determine this mean *Rd* value for *in vivo* human sino-nasal cavities. This mean *Rd* value can subsequently be used in the determination of the build-up function.

When the build-up function is determined, the optimisation can be performed. The optimisation should be executed for one and for two light sources to determine the best possible outcome. The location of the light source needs to be converted to CT coordinates and the output power needs to be rounded to tens of milliwatts. In the future, the optimisation should be performed using a spherical bulb diffuser and a microlens. The cPDT planning tool should be able to indicate which light sources will lead to the best possible treatment with cPDT.

During the treatment, the light source needs to be placed on the planned location. This can possibly be done using an electromagnetic (EM) navigation system that is already available at the Netherlands Cancer Institute Amsterdam: the Fusion Ear, Nose and Throat (ENT) surgical navigation system (Medtronic, Minneapolis, Minnesota, https://www.medtronic.com). The planned light source location can be indicated in the CT scan and this can be loaded into the EM navigation system. The location of some traceable ENT instruments relative to the patient is indicated in the CT scan. The light source is attached to a flexible fiber and it is not possible to trace its location. Therefore, the light source should be fixed to a traceable instrument. Ideally, a hollow traceable instrument is used where the light source fits in its lumen, such as a traceable suction tube. However, currently there are no instruments available with a lumen diameter that is big enough to fit the light source. New navigation instruments need to be developed to be able to navigate the light source to the planned location with precision. Alternatively, another navigation system can be used for which hollow traceable instruments are available in which the light source fits.

7 Overall Conclusion

The main goal of this study was to develop a cPDT planning tool for the treatment of superficial sino-nasal carcinomas. This planning tool should be able to calculate the OSL and its output power ensuring a constant quality of the treatment. Currently, the light source location and its output power are based on intuition and basic dosimetric calculations. When the source location and its output power is calculated based on a light distribution model, it is expected that the clinical outcomes will improve and less side effects will occur.

The first sub-goal was to improve the quality of the empirical light distribution model by evaluating the build-up function. The measurements done in this study showed that it is not correct to describe the build-up function with a linear equation. A quadratic relation between the β factor and the distance from the light source to the surface is found. Subsequently, this quadratic function can be predicted when the size of the cavity and Rd are known. More research should be done to confirm the relations that are found in this thesis.

The second sub-goal was to develop an optimisation algorithm that is able to calculate the OSL and its output power. There is found that a differential evolution algorithm with a population size of 25, mutation constant of (0.75, 1) and a crossover probability constant of 0.6 can be used for the cPDT planning tool. This optimisation algorithm gives an OSL and its output power for multiple light sources within a reasonable time frame and with minimal variations between multiple measurements. The main drawback of the currently developed planning tool is that the algorithm does not take shaded areas into account and that only a spherical bulb diffuser can be used. Therefore, the first step towards the implementation of a microlens in the light distribution models is made in this thesis. The first algorithm is created, but its accuracy needs to be tested in further research.

A Additional figures

A.1 | Variation of objective function

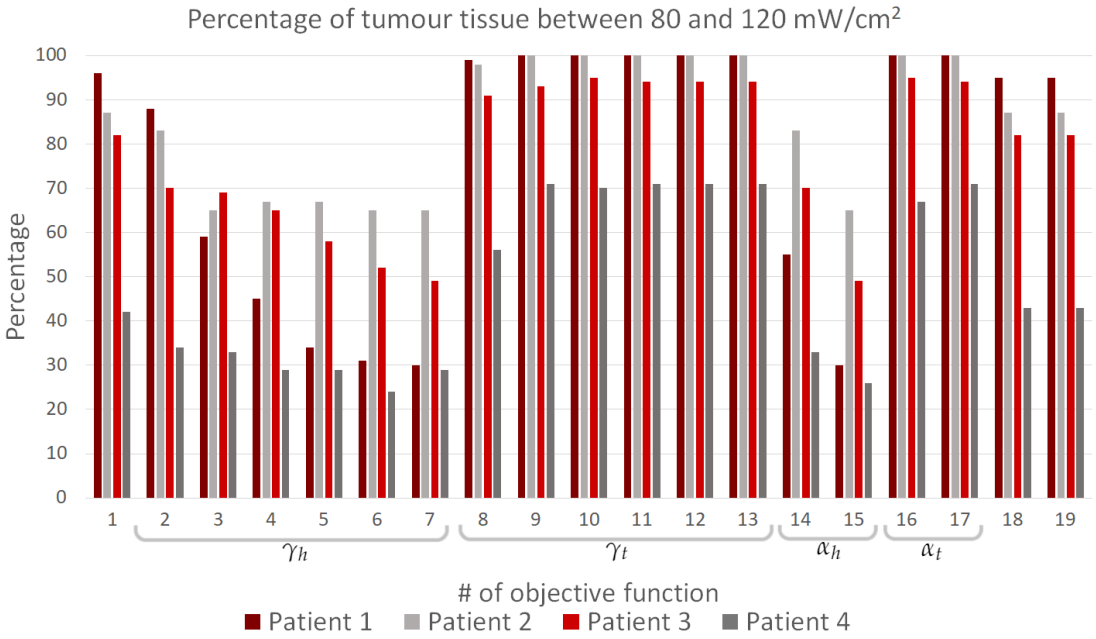

Figure A.1: Percentage of tumour tissue with a fluence rate between 80 and 120 mW/cm^2 for 19 objective functions for all four patients. The variable in the objective function is indicated below the number of the objective function.

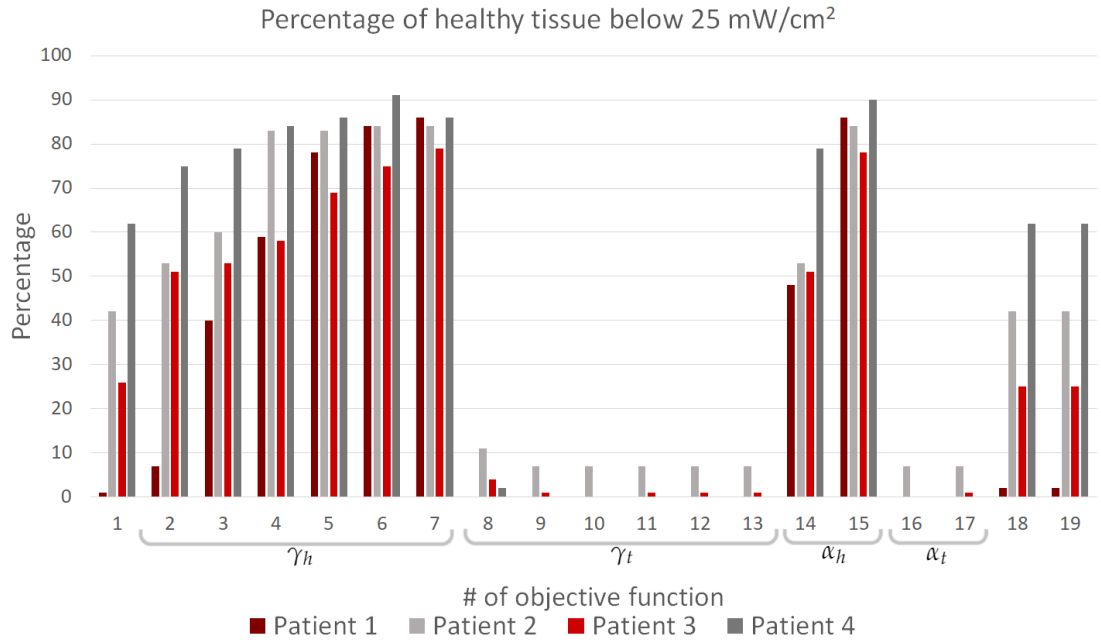

Figure A.2: Percentage of healthy tissue with a fluence rate below 25 mW/cm^2 for 19 objective functions for all four patients. The variable in the objective function is indicated below the number of the objective function.

A.2 | Delineation of tumour

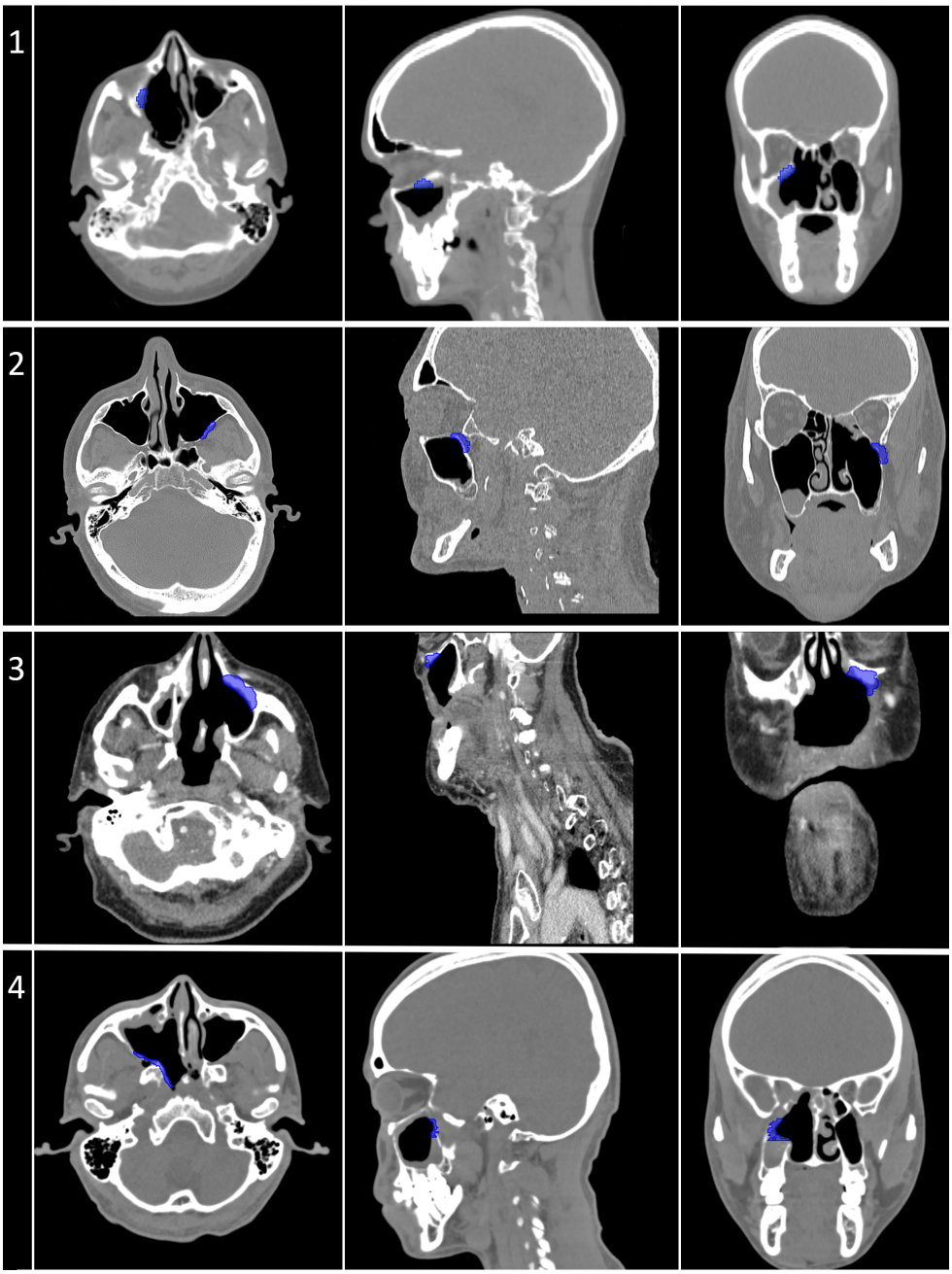

Figure A.3: Delineation of the tumour (blue) in the CT scans of the four patients.

Bibliography

[1] A. Singh, C. Massey and A. Meyers, *Paranasal sinus anatomy*, 2017. [Online]. Available: https://www.cancer.gov/publications/dictionaries/cancer-terms/def/paranasal-sinus (visited on 25/01/2019).

[2] L. Schlossberg and G. Zuidema, *The Johns Hopkins Atlas of Human Functional Anatomy*. Johns Hopkins University Press, 1997.

[3] W. Dauber, H. Feneis and A. Gribnau, *Feneis' Geïllustreerd anatomisch zakwoordenboek*, 4th. Bohn Stafleu van Loghum, 2006, pp. 166–167.

[4] K. Moore, A. Dalley and A. Agur, *Clinically Oriented Anatomy*, 7th ed., ser. Clinically Oriented Anatomy. Wolters Kluwer Health, Lippincott Williams & Wilkins, 2013, pp. 960–963.

[5] J. Keir, "Why do we have paranasal sinuses?", *The Journal of Laryngology & Otology*, vol. 123, no. 1, pp. 4–8, 2009.

[6] J. Llorente, F. López, C. Suárez and M. Hermsen, "Sinonasal carcinoma: clinical, pathological, genetic and therapeutic advances", *Nature Reviews Clinical Oncology*, vol. 11, no. 8, pp. 460–472, 2014.

[7] *Integraal kankercentrum Nederland (IKNL). Cijfers over kanker.* [Online]. Available: https://www.cijfersoverkanker.nl/ (visited on 21/01/2019).

[8] A. Binazzi, P. Ferrante and A. Marinaccio, "Occupational exposure and sinonasal cancer: A systematic review and meta-analysis", *BMC Cancer*, vol. 15, no. 1, 2015.

[9] S. Syrjanen, "The role of human papillomavirus infection in head and neck cancers", *Annals of Oncology*, vol. 21, no. 7, pp. vii243–vii245, 2010.

[10] R. de Bree, C. van Laer, M. van den Brekel and C. Leemans, "Oncologie", in *Leerboek keel-neus-oorheelkunde en hoofd-halschirurgie*, 2nd ed., 2013, ch. 24, pp. 377–378.

[11] J. Turner and D. Reh, "Incidence and survival in patients with sinonasal cancer: a historical analysis of population-based data.", *Head & neck*, vol. 34, no. 6, pp. 877–885, 2012.

[12] R. Carrau, Y. Ong, C. Solares, F. Talavera, N. Sadeghi, A. Meyers and W. Lydiatt, *Malignant Tumors of the Nasal Cavity*, 2017. [Online]. Available: `https://emedicine.medscape.com/article/846995` (visited on 21/01/2019).

[13] J. Tobias and D. Hochhauser, *Cancer of the head and neck*. Wiley, 2014, pp. 173–174.

[14] R. Wong and D. Kraus, *Cancer of the nasal cavity and paranasal sinuses*, ser. American Cancer Society atlas of clinical oncology. American Cancer Society Atlas of Clinical Oncology, BC Decker, 2001, ch. 11, pp. 204–210.

[15] J. Shah and S. Patel, *Cancer of the Head and Neck*. American Cancer Society Atlas of Clinical Oncology, BC Decker, 2001.

[16] M. Amin, S. Edge, F. Greene, D. Byrd, R. Brookland, M. Washington, J. Gershenwald, C. Compton, K. Hess and D. Sullivan, *AJCC Cancer Staging Manual*, 7th ed. Springer International Publishing, 2018, pp. 69–73.

[17] P. Ene, R. C. Popescu, S. Voiculescu, R. Scaunasu, B. Popescu, R. Grigore, R. Ene and C. Cârstoiu, "Sentinel lymph node - work hypothesis in sinonasal carcinoma treatment.", *Maedica*, vol. 6, no. 4, pp. 308–12, 2011.

[18] P. Agostinis, K. Berg, K. A. Cengel, T. H. Foster, A. W. Girotti, S. O. Gollnick, S. M. Hahn, M. R. Hamblin, A. Juzeniene, D. Kessel, M. Korbelik, J. Moan, P. Mroz, D. Nowis, J. Piette, B. C. Wilson and J. Golab, "Photodynamic therapy of cancer: An update", *CA: A Cancer Journal for Clinicians*, vol. 61, no. 4, pp. 250–281, 2011.

[19] D. van Straten, V. Mashayekhi, H. de Bruijn, S. Oliveira and D. Robinson, "Oncologic Photodynamic Therapy: Basic Principles, Current Clinical Status and Future Directions", *Cancers*, vol. 9, no. 12, p. 19, 2017.

[20] *Realtime PDT Dosimetry | Atomic Physics*. [Online]. Available: `http://www.atomic.physics.lu.se/biophotonics/research/photodynamic-therapy/realtime-pdt-dosimetry/` (visited on 22/01/2019).

[21] "European Medicines Agency, Foscan: EPAR - Product information", EMA, Tech. Rep., 2016, pp. 1–28.

[22] F. Civantos, B. Karakullukcu, M. Biel, C. Silver, A. Rinaldo, N. Saba, R. Takes, V. Vander Poorten and A. Ferlito, "A Review of Photodynamic Therapy for Neoplasms of the Head and Neck", *Advances in Therapy*, vol. 35, pp. 324–340, 2018.

[23] K. Plaetzer, B. Krammer, J. Berlanda, F. Berr and T. Kiesslich, "Photophysics and photochemistry of photodynamic therapy: Fundamental aspects", *Lasers in Medical Science*, vol. 24, no. 2, pp. 259–268, 2009.

[24] T. Dai, B. Fuchs, J. Coleman, R. Prates, C. Astrakas, T. St. Denis, M. Ribeiro, E. Mylonakis, M. Hamblin and G. Tegos, "Concepts and principles of photodynamic therapy as an alternative antifungal discovery platform", *Frontiers in Microbiology*, vol. 3, pp. 1–16, 2012.

[25] R. L. P. van Veen, H. Nyst, S. Rai Indrasari, M. Adham Yudharto, D. J. Robinson, I. B. Tan, C. Meewis, R. Peters, S. Spaniol, F. A. Stewart, P. C. Levendag and H. J.C. M. Sterenborg, "In vivo fluence rate measurements during Foscan[sup ®]-mediated photodynamic therapy of persistent and recurrent nasopharyngeal carcinomas using a dedicated light applicator", *Journal of Biomedical Optics*, vol. 11, no. 4, 2006.

[26] Industrial-buy, *Photodynamic Therapy*. [Online]. Available: `https://industrialbuy.com/photodynamic-therapy.html` (visited on 22/01/2019).

[27] Á. Juarranz, P. Jaén, F. Sanz-Rodríguez, J. Cuevas and S. González, "Photodynamic therapy of cancer. Basic principles and applications", *Clinical and Translational Oncology*, vol. 10, no. 3, pp. 148–154, 2008.

[28] A. Kübler, M. Scheer and J. Zöller, "Photodynamic Therapy of Head and Neck Cancer", *Onkologie*, vol. 24, pp. 230–237, 2001.

[29] R. Allison and K. Moghissi, "Photodynamic therapy (PDT): PDT mechanisms", *Clinical Endoscopy*, vol. 46, no. 1, pp. 24–29, 2013.

[30] E. Reginato and P. Wolf, "Immune response after photodynamic therapy increases anti-cancer and anti-bacterial effects", *World Journal of Immunology*, vol. 4, no. 1, pp. 1–11, 2014.

[31] T. van Doeveren., R. Bouwmans, N. Wassenaar, W. Schreuder, M. van Alphen, F. van der Heijden, I. B. Tan, M. B. Karakullukcu and R. van Veen, "On the Development of a Light Dosimetry Planning Tool for Photodynamic Therapy in Arbitrary Shaped Cavities: Initial Results", *Photochemistry and Photobiology*, 2019.

[32] R. Bouwmans, "Intra-cavity light distribution model for photodynamic therapy", PhD thesis, 2019.

[33] Medlight SA, *Medlight Spherical light diffuser*, 2015.

[34] S. Keereweer, P. B. Van Driel, T. J. Snoeks, J. D. Kerrebijn, R. J. De Jong, A. L. Vahrmeijer, H. J. Sterenborg and C. W. Löwik, "Optical image-guided cancer surgery: Challenges and limitations", *Clinical Cancer Research*, vol. 19, no. 14, pp. 3745–3754, 2013.

[35] W. M. Star, "Light delivery and light dosimetry for photodynamic therapy", *Lasers in Medical Science*, vol. 5, no. 2, pp. 107–113, 1990.

[36] N Noe and M. Rety, "Improved Coupled Radiosity & Ray-Tracing Method for Mid and High Frequencies Pass-By Noise Prediction", 2018.

[37] F. van der Heijden, *Image Based Measurement Systems: Object Recognition and Parameter Estimation*, ser. Design and measurement in electronic engineering. Wiley, 1994, p. 14.

[38] L. Caesar, T. E. van Doeveren, I. B. Tan, A. Dilci, R. L. van Veen and B. Karakullukcu, "The use of photodynamic therapy as adjuvant therapy to surgery in recurrent malignant tumors of the paranasal sinuses", *Photodiagnosis and Photodynamic Therapy*, vol. 12, no. 3, pp. 414–421, 2015.

[39] C. Hopper, A. Kübler, H. Lewis, I. B. Tan, G. Putnam, T. Patrice, C. Beauvillain, J. Evensen, K. Butow, B. Smit, J. Brown, J. De Carpentier, J. Carruth, M. Dilkes, G. Kenyon, F. Roberts and N. Sudderick, "mTHPC-mediated photodynamic therapy for early oral squamous cell carcinoma", *International Journal of Cancer*, vol. 111, no. 1, pp. 138–146, 2004.

[40] T. E. van Doeveren, M. B. Karakullukçu, R. L. van Veen, M. Lopez-Yurda, W. H. Schreuder and I. B. Tan, "Adjuvant photodynamic therapy in head and neck cancer after tumor-positive resection margins", *Laryngoscope*, vol. 128, no. 3, pp. 657–663, 2018.

[41] A Master, A Malamas, R Solanki, D. M. Clausen, J. L. Elseman and A. S. Gupta, "Optimization of a Nanomedicine Strategy for Cell-Targeted Photodynamic Therapy of Head- & -Neck Cancers", vol. 10, no. 5, pp. 1988–1997, 2011.

[42] H. Kataoka, H. Nishie, N. Hayashi, M. Tanaka, A. Nomoto, S. Yano and T. Joh, "New photodynamic therapy with next-generation photosensitizers", *Annals of Translational Medicine*, vol. 5, no. 8, pp. 1–7, 2017.

[43] N. Betrouni, C. Munck, W. Bensoltana, G. Baert, A. S. Dewalle-Vignion, A. Scherpereel and S. Mordon, "Real-time light dosimetry for intra-cavity photodynamic therapy: Application for pleural mesothelioma treatment", *Photodiagnosis and Photodynamic Therapy*, vol. 18, pp. 155–161, 2017.

[44] J. Sandell, C. Chang, J. C. Finlay and T. C. Zhu, "A treatment planning system for pleural PDT", *SPIE*, vol. 7551, no. March 2010, 2010.

[45] T. C. Zhu, M. M. Kim, X. Liang, B. Liu, J. L. Meo, J. C. Finlay, A. Dimofte, C. Rodriguez, C. Simone, K. Cengel and J. Friedberg, "Real-time treatment feedback guidance of Pleural PDT", *SPIE*, vol. 8568, no. March 2013, 2013.

[46] T. C. Zhu, M. M. Kim, S. L. Jacques, R. Penjweini, A. Dimofte, J. C. Finlay, C. B. Simone, K. A. Cengel and J. Friedberg, "Real-time treatment light dose guidance of Pleural PDT: an update", *SPIE*, vol. 9308, no. March 2015, 2015.

[47] B. Karakullukcu, S. D. Stoker, A. P. E. Wildeman, M. P. Copper, M. A. Wildeman and I. B. Tan, "A matched cohort comparison of mTHPC-mediated photodynamic therapy and trans-oral surgery of early stage oral cavity squamous cell cancer", *European Archives of Oto-Rhino-Laryngology*, vol. 270, no. 3, pp. 1093–1097, 2013.

[48] C. Dupont, G. Baert, S. Mordon and M. Vermandel, "Parallelized Monte-Carlo dosimetry using graphics processing units to model cylindrical diffusers used in photodynamic therapy: From implementation to validation", *Photodiagnosis and Photodynamic Therapy*, vol. 26, no. December 2018, pp. 351–360, 2019.

[49] E. Oakley, B. Wrazen, D. A. Bellnier, Y. Syed, H. Arshad and G. Shafirstein, "A new finite element approach for near real-time simulation of light propagation in locally advanced head and neck tumors", *Lasers in Surgery and Medicine*, vol. 47, no. 1, pp. 60–67, 2015.

[50] T. M. Baran and T. H. Foster, "Comparison of flat cleaved and cylindrical diffusing fibers as treatment sources for interstitial photodynamic therapy", *Medical Physics*, vol. 41, no. 2, pp. 1–8, 2014.

[51] T. M. Baran, D. P. Nazareth and T. H. Foster, "Image-guided treatment planning and dosimetry for interstitial photodynamic therapy", *Biomedical Optics*, pp. 3–5, 2012.

[52] A. Fedorov, R. Beichel, J. Kalpathy-Cramer, J. Finet, J.-C. Fillion-Robin, S. Pujol, C. Bauer, D. Jennings, F. Fennessy, M. Sonka, J. Buatti, S. Aylward, J. V. Miller, S. Pieper and R. Kikinis, "3D Slicer as an image computing platform for the Quantitative Imaging Network", *Magnetic resonance imaging*, vol. 30, no. 9, pp. 1323–1341, 2012.

[53] U. Oelfke, S. Nill and J. J. Wilkens, "Physical optimization", in *Image-Guided IMRT*, 2006, pp. 31–45.

[54] J. Pintér and J. Szabó, "Global optimization algorithms: Theory and some applications", *System Modelling and Optimization*, pp. 704–713, 2006.

[55] M. S. Khan, I. A. Karimi and D. A. Wood, "Retrospective and future perspective of natural gas liquefaction and optimization technologies contributing to efficient LNG supply: A review", *Journal of Natural Gas Science and Engineering*, vol. 45, pp. 165–188, 2017.

[56] K Price, R. M. Storn and J. A. Lampinen, *Differential Evolution: A Practical Approach to Global Optimization*, ser. Natural Computing Series. Springer Berlin Heidelberg, 2006, pp. 30–34.

[57] E. L. Melnick and B. S. Everitt, *Encyclopedia of Quantitative Risk Analysis and Assessment*, ser. Encyclopedia of Quantitative Risk Analysis and Assessment. John Wiley & Sons, 2008, pp. 969–972.

[58] Y. Gao, "Population Size and Sampling Complexity in Genetic Algorithms", *Proceedings for the bird of a feather workshops*, pp. 178–181, 2003.

[59] SciPy, *Optimization scipy*. [Online]. Available: `https://docs.scipy.org/doc/scipy/reference/tutorial/optimize.html` (visited on 06/11/2019).

[60] P. Kaelo and M. M. Ali, "A numerical study of some modified differential evolution algorithms", *European Journal of Operational Research*, vol. 169, no. 3, pp. 1176–1184, 2006.

[61] E Mezura-Montes, J Velazquez-Reyes and C. A. C. Coello, "Modified Differential Evolution for Constrained Optimization", in *2006 IEEE International Conference on Evolutionary Computation*, 2006, pp. 25–32.

[62] M. Ali, P. Siarry and M. Pant, "An efficient Differential Evolution based algorithm for solving multi-objective optimization problems", *European Journal of Operational Research*, vol. 217, no. 2, pp. 404–416, 2012.

[63] Medlight SA, *Medlight Frontal light distributor*, 2015.

[64] Medlight SA, *Medlight optical endoscopic illumination*. [Online]. Available: `www.medlight.com` (visited on 05/11/2019).

[65] I. B. Tan, H. Oppelaar, M. C. Ruevekamp, R. B. Veenhuizen, A. Timmers and F. A. Stewart, "The importance of in situ light dosimetry for photodynamic therapy of oral cavity tumors", *Head and Neck*, vol. 21, no. 5, pp. 434–441, 1999.

[66] R. A. Weersink, J. Qiu, A. J. Hope, M. J. Daly, B. C. Cho, R. S. Dacosta, M. B. Sharpe, S. L. Breen, H. Chan and D. A. Jaffray, "Improving superficial target delineation in radiation therapy with endoscopic tracking and registration", *Medical Physics*, vol. 38, no. 12, pp. 6458–6468, 2011.